AD-A146 641 THEORETICAL INVESTIGATION OF DEVICE ASPECTS OF SEMICONDUCTOR SUPERLATTICES(U) MAX-PLANCK-INST FUER FETTKOERPERFORSCHUNG STUTTGART (GERMANY F.. 1/1

UNCLASSIFIED G H DOEHLER SEP 83 R/D-3092-EE F/G 20/2 NL

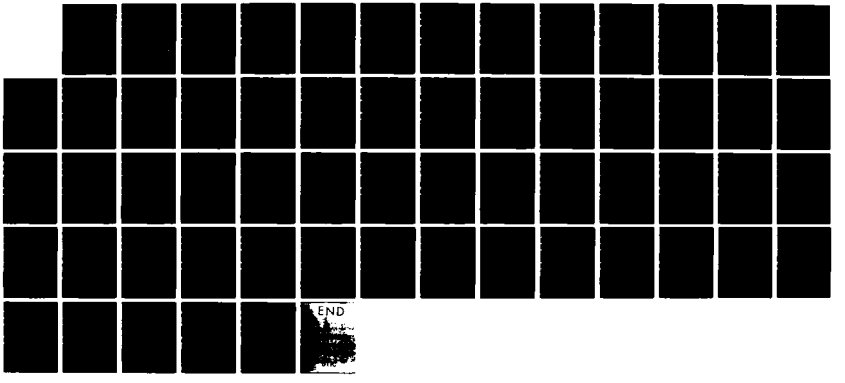

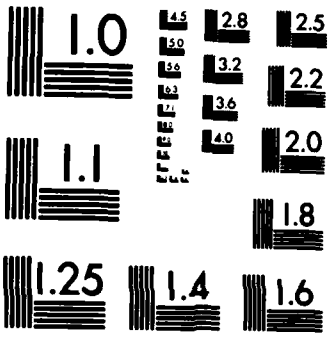

MICROCOPY RESOLUTION TEST CHART
NATIONAL BUREAU OF STANDARDS-1963-A

UNCLASSIFIED

SECURITY CLASSIFICATION OF THIS PAGE (When Data Entered)

R&D 3092-EE

(7)

REPORT DOCUMENTATION PAGE		READ INSTRUCTIONS BEFORE COMPLETING FORM
1. REPORT NUMBER	2. GOVT ACCESSION NO.	3. RECIPIENT'S CATALOG NUMBER
4. TITLE (and Subtitle) Theoretical Investigation of Device Aspects of Semiconductor Superlattices		5. TYPE OF REPORT & PERIOD COVERED Final Technical Report March 81 - June 82
		6. PERFORMING ORG. REPORT NUMBER
7. AUTHOR(s) Gottfried H. Döhler		8. CONTRACT OR GRANT NUMBER(s) DAJA37-81-C-0191
9. PERFORMING ORGANIZATION NAME AND ADDRESS Max-Planck-Institut für Festkörperforschung Stuttgart 80, Germany		10. PROGRAM ELEMENT, PROJECT, TASK AREA & WORK UNIT NUMBERS 6.11.02A IT161102BH57-03
11. CONTROLLING OFFICE NAME AND ADDRESS USARDSG-UK Box 65, FPO NY 09510		12. REPORT DATE Sept 1983
		13. NUMBER OF PAGES 53
14. MONITORING AGENCY NAME & ADDRESS (if different from Controlling Office)		15. SECURITY CLASS. (of this report) Unclassified
		15a. DECLASSIFICATION/DOWNGRADING SCHEDULE

16. DISTRIBUTION STATEMENT (of this Report)

Approved for public release; distribution unlimited

17. DISTRIBUTION STATEMENT (of the abstract entered in Block 20, if different from Report)

18. SUPPLEMENTARY NOTES

19. KEY WORDS (Continue on reverse side if necessary and identify by block number)

semicondutors, superlattices, GaAs, III-V compounds, negative differential conductivity, microwave generation, Gunn oscillators, FIR, IR detectors, tunable light sources, tunable laser, FIR laser, optical modulators, ultrafast, ultrasensitive.

20. ABSTRACT (Continue on reverse side if necessary and identify by block number)

Semiconductor superlattices are synthetic crystals, which consist either of a periodic sequence of ultrthin layers of two different semiconductors ("compositional superlattices") or of a single homogeneous semiconductor, which is periodically n- and p- doped, possibly with intrinsic layers in between ("n-i-p-i crystals"). I have investigated electrical and electro-optical device applications of semiconductor superlattices in general, but with special emphasis on fast devices and oscillators for

DD FORM 1 JAN 73 1473 EDITION OF 1 NOV 65 IS OBSOLETE

UNCLASSIFIED

SECURITY CLASSIFICATION OF THIS PAGE (When Data Entered)

20 (Continued)

microwave generation. It is found, that an extremely wide spectrum of possibilities results from the fact that the properties of superlattices can be tailored for a given goal. I have considered two groups of device applications according to the two major classes of semiconductor superlattices:
i) Devices, which rely on properties, which are in common to both classes of superlattices. The most appealing devices in this class are the FIR lasers, based on stimulated emission associated with interlayer transitions.
ii) Devices, which rely on the unique features of the doping superlattices. The electronic properties of these superlattices cannot only be tailored but they can be "tuned" within wide limits for a given specimen. Moreover, the electron-hole recombination lifetimes ecceed those of the host materials by many orders of magnitude. Novel n-i-p-i devices include bulk field effect transistors, ultrasensitive or ultrafast IR photodetectors, tunable light-emitting devices, and ultrafast optical modulators. Particularly appealing aspects of n-i-p-i device applications are the possibility to start from nearly any semiconductor as host material and the rather modest requirements for purity and perfection of the crystals.

THEORETICAL INVESTIGATION OF DEVICE ASPECTS OF SEMICONDUCTOR SUPERLATTICES

Final Technical Report

by

Gottfried H. Döhler

September 1983

United States Army
EUROPEAN RESEARCH OFFICE OF THE U.S. Army
London England
Contract Number: DAJA37-81-C-0191
Contractor: Dr. Gottfried H. Döhler

Approved for Public Release; distribution unlimited

Summary

Semiconductor superlattices are synthetic crystals, which consist either of a periodic sequence of ultrthin layers of two different semiconductors ("compositional superlattices") or of a single homogeneous semiconductor, which is periodically n- and p- doped, possibly with intrinsic layers in between ("n-i-p-i crystals"). The author investigated electrical and electro-optical device applications of semiconductor superlattices in general, but with special emphasis on fast devices and oscillators for microwave generation. It is found, that an extremely wide spectrum of possibilities results from the fact that the properties of superlattices can be tailored for a given goal. I have considered two groups of device applications according to the two major classes of semiconductor superlattices:
i) Devices, which rely on properties, which are in common to both classes of superlattices. The most appealing devices in this class are the FIR lasers, based on stimulated emission associated with interlayer transitions.
ii) Devices, which rely on the unique features of the doping superlattices. The electronic properties of these superlattices cannot only be tailored but they can be "tuned" within wide limits for a given specimen. Moreover, the electron-hole recombination lifetimes ecceed those of the host materials by many orders of magnitude. Novel n-i-p-i devices include bulk field effect transistors, ultrasensitive or ultrafast IR photodetectors, tunable light-emitting devices, and ultrafast optical modulators. Particularly appealing aspects of n-i-p-i device applications are the possibility to start from nearly any semiconductor as host material and the rather modest requirements for purity and perfection of the crystals.

Keywords:

semicondutors, superlattices, GaAs, III-V compounds, negative differential conductivity, microwave generation, Gunn oscillators, FIR, IR detectors, tunable light sources, tunable laser, FIR laser, optical modulators, ultrafast, ultrasensitive.

Table of Contents

PREAMBLE

The period of the investigation reported here coincides with a rather unusual situation for the investigator. His work on doping superlattices, initiated by the investigator twelve years ago and performed by him and his coworkers, turned out more and more successful during the last three years and received increasing recognition by the physical community. This special situation had 3 major effects on his work on this investigation of device aspects of semiconductor superlattices:

1) The periodical reports and, in particular, the final report were delayed. This was due to the investigator being strongly involved in the work in progress on n-i-p-i doping superlattices, with numerous invitations for International Conferences, Seminars and Colloquia and, last not least, the preparation of original papers and review articles on this subject. I apologize sincerely for this delay.

2) In my proposal for this investigation there was, still implicitely, a certain emphasis on doping superlattices apparent. The progress during the last two years has further corroborated my personal opinion , that doping superlattices represent a more flexible and powerful basic material for semiconductor device applications than their compositional counterparts. Consequently, my activities were concentrated on the device aspects of the doping superlattices (although the number of pages devoted to compositional superlattices in this report does not reflect this fact. In contrast to the work on doping superlattices, the results on compositional superlattices have not yet been published).

3) Both, the progress of research in this field, but also the delay of this final report result in a number of new results and proposals for device applications which were not anticipated or might have appeared too phantastic still a few years ago.

1. INTRODUCTION

In my proposal for this investigation it was mentioned that claims for possible device applications had been made in connection with the first theoretical investigations of semiconductor superlattices by several authors. I also mentioned that, apart from those claims, little detailed investigations, neither theoretical nor experimental, had been done. Apart from a few singular exceptions (to be mentioned below) the situation has not changed substantially within the three years which have passed in the mean time. This observation is particularly surprising in view of the growing interest of solid state physicists in the field of superlattices and other sub-micron structures. Several explanations for this phenomenon are principally possible:

1) The claims of the above mentioned authors were not correct, not serious, too academic, not taking into account the problems occuring in the real world of semiconductors.

2) The properties investigated by these athors appeared not attractive enough for stimulating device oriented people to work on the subject.

3) We have now reached a state of the art which allows us to work out the fundamental theory of superlattice phenomena and to verify the theoretical predictions by experiments. The literature of the last few years gives an impressive record of this development /1/. Researchers working in this field investigate new materials, new techniques and find new phenomena, expected, but also unexpected ones. The introduction of modulation doping /2,1/, of the quantum Hall effect /3,1/, and the work on doping superlattices /4-7,1/ may serve as examples. Most of the physicists working in the field are mainly concerned with the basic physical phenomena. They do not worry adequately about device implications, which they may just mention occasionally.

4) Most of the properties of semiconductor superlattices are too exotic (or, at least, too unusual). Semiconductor superlattices do not represent simply a new (or better) basic material for the fabrication of improved conventional devices (with, perhaps, a few exceptions). The true potential of semiconductor superlattices lies in their use for novel devices. Therefore, it happens that most of the experimental device physicists are not sufficiently aware of those peculiarities of semiconductor superlattices which make them attractive for device applications. This assertion can be supported by one of the few examples where the interest for device applications of superlattices (actually not a superlattice, but rather a heterostructure) has been evident in terms of conventional devices. This example is the concept of modulation doping, yielding extremely high carrier mobilities /2/.

The impact of this discovery on device scientists was so strong, that, by now, apart from many non-profit research institutions most of the major industrial research laboratories all over the world are working on the development of ultrafast high-speed transistors using modulation doped heterostructures (HEMT's /8,9/, or 2-DEG MESFET's /10,9/).

While the arguments 1) and 2) are not correct in my opinion (there may have been some too optimistic speculations, occasionally, with respect to point 1), but point 2) is certainly not correct), the points 3) and 4), together, provide a reasonable and consistent view of the present situation. I would like to express my general view, in particular after this study, by saying that we are now reaching the level at which device applications of semiconductor superlattices can and should be considered seriously:

1) A high technological level in growing superlattices with well-defined design has been accomplished.

2) The experimental results on such sophisticated structures provide sound confidence not only concerning the feasibility of making the structures, but also into the correctness of the basic theoretical concepts. Thus, we are encouraged to make use of the novel properties of such materials also for the fabrication of novel devices.

The purpose of this theoretical investigation is to encourage and to stimulate device experts to make use of semiconductor superlattices where it appears promising from the theoretical point of view. But we will also try to address problems associated with some interesting new ideas or concepts, which appear attractive, but may not be feasible or really useful in practice.

The range of potential device applications of semiconductor superlattices covers nearly the whole field of electronic and opto-electronic devices and could not be investigated in depth in the framework of this study. In this report I will first give a brief summary of the specific features of semiconductor superlattices and of the basic quantitative relations between the "design" parameters and those features (Section 2). In sections 3) and 4) we will investigate those electronic properties of semiconductor superlattices which make them suitable and attractive for device applications. The complexity of features and resulting possible applications causes considerable difficulties in ordering those aspects systematically. As the most practical way to subdivide this discussion into classes of properties appears distinguishing between features which are specific for superlattices in general, but <u>not specific</u> for doping superlattices (but may be exhibited by those,

as well as by their compositional counterparts!) (section 3), and those which exclusively occur in doping superlattices (section 4).

The major part of the latter section has been included in papers which have either been published recently or are in press. Therefore, this part of the study will be summarized only in this report. Most of the results reported in section 3 have not yet been published (though publication is anticipated). They will be presented here in more detail. Thus, the space devoted to various topics in this report is not at all related to the significance which I attribute to each of them!

2. Summary of the electronic properties of semiconductor superlattices.

A semiconductor superlattice is a periodic sequence of ultrathin layers which differ from each other either by their composition ("heterojunction superlattices", or "compositional superlattices") or by the sign of doping ("homojunction superlattices, "p-n-junction superlattices, or "n-i-p-i crystals"). A brief review of their properties is given under Ref. /11/, a more detailed one in /12/. For the understanding of this report it will be sufficient if we summarize a few features. Some of these features are in common to all kinds of semiconductor superlattices, but others are specific for doping superlattices only.

2.1. Superlattice potential

The strongly modified properties of semiconductor superlattices are a consequence of the superlattice potential which results from the variation in composition or doping. Figs. 1 - 4 exhibit 4 major possibilities :

a) Compositional superlattice, type I (Fig.1). (Example: s.c.^{I}: GaAs, s.c.^{II}: $Al_xGa_{1-x}As$). The band gaps of the two components differ by an amount

$$V_o = E_g^{II} - E_g^{I}$$

The discontinuity of the band edges in the conduction and the valence band $V_{o,c}$ and $V_{o,v}$ creates a strong, rectangular shaped potential in the conduction and the valence bands.

b) compositional superlattice, type II (Fig.2). (Example: s.c.^{I}: InAs, s.c.^{II}: GaSb). Type II differs from type I by the sign of the band edge discontinuities:

Type I: opposite sign
Type II: same sign
} for conduction and valence band discontinuities

c) Doping superlattice (n-i-p-i) (Fig.3). Example: GaAs with Si-donors and Be-acceptors). The space-charge potential of the impurities acts as the superlattice potential.
Example: $d_D = d_D$; $n_D = n_A$; $d_i = 0$, i.e. no intrinsic layers (the term n-i-p-i crystal" is also used for doping superlattices which do not contain intrinsic layers in their periodic sequence of layers).
Amplitude of the superlattice potential:

$$V_o = (2\pi e^2 n_D / \kappa_o)(d_m/2)^2 \qquad (1)$$

Important: Parallel modulation of conduction and valence band edge by superposition of the space charge potential to the crystal potential. Any value of V_o up to $E_g^{\delta}/2$ can be achieved by appropriate choice of design parameters.

d) Hetero-doping superlattice. (Example: $Al_xGa_{1-x}As$ n-i-p-i, with intercallated intrinsic GaAs layers) (Fig.4). The superlattice potential originates from band gap discontinuities and space charge fields /11/.

2.2. Electronic structure of semiconductor superlattices.

The electronic structure of semiconductor superlattices differs very strongly from the electronic structure of a uniform semiconductor:

a) The electronic properties are highly anisotropic: Propagation of the carriers in direction of periodicity (denoted as the z-direction in the following) is prohibited if the barriers are wide and high, i.e. the carriers are confined to their layers and can move freely only parallel to the layers.

b) The z-component of the motion in the potential wells is quantized with discrete energy levels labeled $E_{c,\mu}$ (μ= 0, 1, 2, ...) and $E_{v,\nu}$ (ν = 0, 1, 2, ...) for the conduction and valence bands, respectively. Each one of these energies is the edge of a "subband" (see Figs. I-4)

$$\mathcal{E}_{c,\mu}(\vec{k}_{\parallel}) = E_{c,\mu} + (\hbar^2/2m_c)\, k_{\parallel}^2 \qquad (2)$$

$$\mathcal{E}_{v,\nu}(\vec{k}_{\parallel}) = E_{v,\nu} - (\hbar^2/2m_v)\, k_{\parallel}^2 \qquad (3)$$

where the second term on the r.h.s. in (2) and (3) is the kinetic energy for motion parallel to the layers with momentum $\hbar\vec{k}_{\parallel}$. One of the most intriguing features of semiconductor superlattices is the fact that the energy separation between these subbands can be tailored by appropriate choice of the design parameters /11/.

Estimate for type-I compositional superlattices:

$$E_{c,\mu} = E_g^0 + (\hbar^2/2m_c)(\pi/d^I)^2(\mu+1)^2, \text{ if } E_{c,\mu} - E_g^0 < V_c^0 \qquad (4)$$

$$E_{v,\nu} = -(\hbar^2/2m_v)(\pi/d^I)^2(\nu+1)^2, \text{ if } |E_{v,\nu}| < V_v^0 \qquad (5)$$

i.e., the spacing increases linearly with decreasing layer thickness d^I.

Example: GaAs ($m_c = 0.067\ m_0$), $d^I = 10$ nm, $E_{c,0} = 45$ meV

Estimate for doping superlattices /11/:

$$E_{c,\mu} = E_g^0 - 2V_0 + \hbar (4\pi e^2 n_D / \kappa_0 m_c)^{1/2} (\mu + \tfrac{1}{2}), \text{ if } E_{c,\mu} - E_{c,0} < V_0 \quad (6)$$

$$E_{v,\nu} = -\hbar (4\pi e^2 n_A / \kappa_0 m_v)^{1/2}, \text{ if } |E_{v,\nu} - E_{v,0}| < V_0 \quad (7)$$

i.e., the spacing increases with the square root of (doping concentration /(effective mass x dielectric constant)).
Example: GaAs with $n_D = 10^{18} cm^{-3}$, $\kappa_0 = 12.5$, $E_{c,\mu} = E_{c,0} + \mu \times 40$ meV
(Note that d_n and d_p do not affect the subband distances!).

c) With decreasing hights and/or width of the potential barrier separating adjacent potential wells propagation in z-direction becomes possible, because of the interaction between neighboring layers. In other words: the subbands have a finite width with respect to the z-component of the momentum (not shown in Figs I-4):

$$\varepsilon_{c,\mu}(\vec{k}) = \varepsilon_{c,\mu}(\vec{k}_{\parallel}) + V_{c,\mu} \cos k_z z \quad (8)$$

$$\varepsilon_{v,\nu}(\vec{k}) = \varepsilon_{v,\nu}(\vec{k}_{\parallel}) + V_{v,\nu} \cos k_z z \quad (9)$$

In Eqs. (8) and (9) the nearest neighbor tight-binding approximation, which is applicable to nearly all cases of interest, has been used. Estimates for the band width $2V_{c,\mu}$ or $2V_{v,\nu}$ will be given later, in connection with transport in the z-direction. Here we mention only the following: The band width decreases exponentially if the hights and/or the width of the potential barrier between adjacent potential wells increases. Thus, the band width, again, can be tailored by the choice of the design parameters:

For compositional superlattices: The heights V_0^c increases if the Al-content x in the alloy $Al_xGa_{1-x}As$ is increased; the barrier width, of course, is d^{II}.

For doping superlattices: The height $2V_0$ depends on

the design parameters n_D, n_A, d_n, d_p, and d_i, where $2V_o$ follows from Eq. (1) for our simple example. For a given constant value of $2V_o$ the barrier width is proportional to $n_D^{-1/2}$.

e) Tunability of the electronic structure in doping superlattices. This is a unique property of doping superlattices (and hetero-n-i-p-i's) which is exhibited neither by compositional superlattices nor by any uniform semiconductor. The tunability is the key feature for many possible device applications which will be discussed in this report.

A comparison of Figs. 1 - 4 reveals that we have a "direct gap in real space" only in Fig.1, since only in this case the lowest conduction and the uppermost valence band states are confined to the same spatial region, namely to the lower band gap layers. In the Figs. 2 - 4 they are shifted by half a superlattice period, i.e. we are dealing with an "indirect gap in real space". But only in the systems shown in Figs. 3 and 4 the consequences of this indirect gap in real space turn out to be dramatic. There are three major consequences which result from the strong spatial separation between electrons and holes.

1) Tunability of the carrier concentration. If there are charge carriers in the subbands (we will show later on how one can populate these subbands) the electron states exhibit only an exponentially small overlap with the hole states (see the lowest subband wave functions indicated schematically in Fig. 3 and 4). Therefore, the electron-hole recombination lifetimes will be very large. How large they are actually depends on the width and the hight of the potential barrier created by the space-charge potential, i.e., it depends first of all on the deign parameters of the doping superlattice. Calculations of the lifetime will be presented later on. The long lifetimes imply that it is possible to maintain large concentrations of excess electrons and holes in the n- and p-layers, respectively, under low excitation or injection conditions. In other words: a situation with different quasi-Fermi-level for electrons, ϕ_n, and for holes, ϕ_p, can be metastable in n-i-p-i crystals.

2) Tunability of the effective band gap. With increasing electron and hole concentration in the n- and p-layers the space charge of the donors and acceptors in the respective layers becomes gradually compensated by the free carriers. The reduction of the amplitude of the space-charge potential yields an increase of the effective band gap ($E_g^{eff,o} \rightarrow E_g^{eff,n}$, see Figs. 3a and b and 4a and b).

3) Tunable lifetime. The lifetimes for excess carriers decrease extremely when $E_g^{eff,n}$ increases, since the overlap between occupied subbands increases, or, once more in other words, since the tunneling barrier for electron-hole recombination becomes flatter and narrower (compare Figs. 3a and b). We will discuss this effect in detail later on.

In the next two sections of this report we will list and discuss electronic properties which are specific for superlattices and which appear attractive for device applications. In order to obtain some systematics a distinction will be made between properties which are in common to compositional and doping superlattices (section 3) and others, which are exclusively shown by doping superlattices, i.e. n-i-p-i crystals and hetero n-i-p-i's (section 4).

3. Properties, not specific for doping superlattices.

Because of the strong anisotropy of the electronic structure and the anisotropy of the resulting transport properties of superlattices a natural classification scheme for transport phenomena is a distinction between conductivity parallel to the layers ($\sigma_{\parallel}$) and normal to them ($\sigma_{\perp}$).

3.1. Transport parallel to the layers.

The transport properties parallel to the layers of a superlattice differ dramatically from the more or less isotropic transport properties of an uniform semiconductor if the concept of modulation doping /2/ is used (see Fig.5). The high mobility observed in modulation-doped superlattices /2,9/ and in hetero-n-i-p-i crystals /11,13/ is an essentially classical superlattice phenomenon. By the simple trick of confining the doping to the more central part of the larger-band-gap material (s.c.^{II} in Figs. 1 and 4) the electrons are spatially separated from the donors, otherwise acting as strong scatterers, since they populate the electronic states of lowest energy, which are confined to the lower-band-gap material (s.c.^{I}). In this way the combination of high carrier concentration and high mobility can coexist in modulation-doped semiconductor superlattices, in contrast to uniformly doped familiar semiconductors. Two device applications of modulation-doped semiconductor heterostructures have been considered in the literature and a third one will be proposed here.

3.1.1. Fast transistors.

A real enthousism among solid state device scientists was the reaction about the reports of extremely high low- and medium-temperature mobilities /9/. They were immediately stimulated to use the new material for ultrafast transistors (see introduction of this report). These transistors are special version of MESFET's (metal semiconductor field effect transistors) with the normal Schottky gate on the n-type GaAs surface layer replaced by a Schottky gate on a selectively doped $Al_xGa_{1-x}As$-GaAs heterojunction. So they are no superlattice devices, but they are only using the same concept of separating electrons

from their parent donors in order to achieve high mobility. Although I will not discuss any details of these high mobility transistors (HEMT /8/) or 2-DEGFET's (= 2-dimensional electron gas FET /10/), I would like to point out that the improvement in performance is by far not so dramatic as it might be expected from the high (low-field !) mobility data of the order of $\mu_o \simeq 10^6\ cm^2V^{-1}s^{-1}$ (at 77K). The actual transit time for a gate length L_x is considerably larger than

$$\tau_t \simeq L_x^2/(\mu_o U_{sd})$$

for usual source-drain voltages U_{sd}. The reason for that is a drastic decrease of mobility with increasing source-drain field $F_{sd} = U_{sd}/L_x$ /14/. This decrease is a consequence of warm and hot carrier effects which become important already at very low fields because of the long relaxation times (Example: A field-independent mobility of $\mu_o = 10^6 cm^2V^{-1}s^{-1}$ implies a momentum relaxation time $\tau_k = \mu m_c/e \simeq 40$ ps. The threshold velocity for the emission of optical phonons is

$$v_{th} = (2\hbar\omega_{LO}/m_c)^{1/2} \simeq 4.4 \times 10^7\ m\,s^{-1}$$

Thus, a field $F = F_{th} = 44\ Vcm^{-1}$ would be sufficient to induce a drift velocity $v_d = \mu_o F$ equal to this threshold velocity! For electric fields of this order of magnitude and above the mobility will be limited by the electron-LO-phonon interaction).

An analysis of measured field-dependent mobilities in terms of electron- LO-phonon scattering, including the effects of screening has been given by Inoue et al. /14/. It should be noted that very favorable transit times are expected for $eU_{sd} \lesssim \hbar\omega_{LO}$ and gate lengths $L_x < \hbar\omega_{LO}/eF_{th} \simeq 8\mu$, if the mobility decreases

only at carrier energies in excess of $\hbar\omega_{LO}$. Under these conditions the transport is ballistic, since the transit time $\tau_t = 2L_x/v_{th}$ becomes shorter than the low-field momentum relaxation time τ_k for $L_x \gtrsim 9\mu$. For a gate length of 1μ, for instance, the transit time becomes at $U_{sd} = \hbar\omega_{LO}/e = 36$ mV

$\tau_t = L_x/(v_{th}/2) \simeq 4.5$ ps.

This short argument implies that the low power consumption of HEMT's (or 2-DEGFET's) may turn out to be even a greater advantage than the gain in switching time.

3.1.2. Real space Gunn oscillators.

Hess has suggested /15/ that the real space transfer of hot electrons in a modulation-doped superlattice from the high-mobility lower-band-gap layers into the low-mobility layers with the larger-band-gap may yield the same effects of domain formation as the inter-valley transfer in momentum space does in the case of the familiar Gunn oscillator.

The theoretical investigation of this phenomenon is extremely difficult. In the case of an $Al_xGa_{1-x}As$- GaAs superlattice, in particular, the energies for real space and momentum intervalley transfer are not sufficiently different to allow for a complete neglect of the latter ones. The question whether the predicted effect may be observable has not yet been answered, neither by theory nor by experiment, although quite some effort has been made. Apart from the problems of the field-dependence of the various momentum-and real-space scattering processes a delicate trade-off between the influences of Al-content x, doping concentration n_D and of the changes of the self-consistent potential due to the real space transfer of electronic charge /16/ has to be considered. It is therefore clear, that a reliable answer to this question is far beyond the scope of this general investigation of superlattice device applications.

3.1.3. High field monochromatic FIR emission.

Radiative inter-subband transitions of hot electrons between subbands in silicon inversion layers have been observed by Gornik et al. /17/ a number of years ago. The same phenomenon occurs in semiconductor superlattices as well. As a matter of fact, the situation is theoretically more favorable for the generation of monochromatic FIR radiation for several reasons:

1) Electrons become hot at rather low fields parallel to the layers, if modulation-doped superlattices are used (See Sect. 3.I.I)

2) The electronic structure can be designed appropriately, in contrast to Si-inversion layers where the subband distances are largely determined by the carrier concentration in the channel.

A favorable electronic structure is shown in Fig. 6a. Such an arrangement of the bands with $E_2 - E_1 \gg E_1 - E_0$, which differs substantially from the results following from the simple expression (4) can be obtained easily if the simple potential wells of Fig. 1 are replaced by potential wells as shown in Fig. 6b (Shown is only the conduction band of this "superlattice with superstructure" for one period of length d).

With increasing thickness $\tilde{d}^{II}$ of the intercallated layer of s.c.^{II}-material the lowest four levels E_0 to E_3 change qualitatively as shown in Fig. 7 ($d^I/2$ and d^{II} being kept constant). At large values of $\tilde{d}^{II}$ the pairs of states (E_0, E_1) and (E_2, E_3) become two-fold degenerate. The spacing between the lowest non-degenerate states becomes by a factor of 4 larger compared with the situation at $\tilde{d}^{II} \rightarrow 0$ because the width of the potential well changes from d^I to $d^I/2$ (see Eq. (4)).

We return to the FIR emission. If $E_2 > \hbar\omega_{LO}$ there will be few electrons in the E_2-band because of the rapid decrease of the hot electron distribution function for

$$\varepsilon_\mu(\vec{k}_\parallel) > E_{c,0} + \hbar\omega_{LO} \qquad (10)$$

3) Furthermore it is favorable to choose a small electron concentration $n^{(2)}$ such that the Fermi energy fulfills the condition

$$\varepsilon_F = (\hbar^2/2m_c)(2\pi n^{(2)}) \ll \hbar\omega_{LO} \tag{11}$$

The hot electron distribution function $f_\mu^h(\varepsilon)$ to lowest order is then

$$f_\mu(\varepsilon) \simeq \begin{cases} \varepsilon_F/(2\hbar\omega_{LO}) \ll 1 \text{ , for } \varepsilon_\mu < E_o + \hbar\omega_{LO} & (12) \\ 0 \text{ , for } \varepsilon_\mu > E_o + \hbar\omega_{LO} & (13) \end{cases}$$

(The factor 2 in the denominator in Eq. (12) takes into account that the electrons are populating two subbands, the lowest and the first excited one). The final states for spontaneous $(1 \rightarrow 0)$-transitions are therefore empty with a probability $1 - f_0(\varepsilon) \simeq 1$ for most of the electrons in the first excited subband.

4) The line width of the emitted FIR radiation with $\hbar\omega = E_1 - E_0$ (see Fig. 6a) should be narrow because of the small subband broadening in modulation-doped superlattices.

5) The intensity is higher than in a single space-charge layer by a factor of N, where N is the number of periods in the superlattice.

The rate of photons emitted per electron and per second is given by

$$w^{sp}_{1\rightarrow 0} = \frac{4}{3}\,\frac{e^2(E_1 - E_0)^3}{\hbar^4 c^3}\,|\vec{r}_{1,0}|^2 \tag{14}$$

The value of the matrixelement $\vec{r}_{1,0}$ can be estimated easily.

$$|\vec{r}_{1,0}| \simeq d^I/2 \tag{15}$$

For $\hbar\omega$ = 10 meV and d^I = 10 nm, for instance, we find

$$w_{1\to 0}^{sp} \simeq 10^4 \ s^{-1} \tag{16}$$

From this result we deduce that the intensity and the efficiency of such a FIR light source will be poor: Estimate for intensity $I(\hbar\omega$ = 10meV): Superlattice of 1 cm^2 area, consisting of 100 periods with a carrier concentration per layer $n^{(2)} = 10^{11} cm^{-2}$.

$$I = 10^2 \times 10^{11} \times 10^4 \times 0.01 \ eVs^{-1} \triangleq 10^{15}/1.6\times 10^{19} watts \simeq 60 \ \mu watt \tag{17}$$

Estimate for efficiency: The emission rate for LO-phonons per electron is of the order of

$$\omega_{LO} \lesssim 10^{12} \ s^{-1} \tag{18}$$

Thus, only a fraction

$$(w_{1\to 0}^{sp} / \omega_{LO})\left(\frac{E_1 - E_0}{\hbar\omega_{LO}}\right) \lesssim 10^{-8} \tag{19}$$

of the total amount of energy dissipated in the device is emitted as FIR radiation. The efficiency could become much higher if there was a possibility to obtain the inter-subband emission in stimulated-emission processes. Unfortunately, we do not see any possibility how to obtain population inversion between the E_1- and E_0-bands in the case of transport parallel to the layers (see, however, the section about transport in z-direction !).

3.2. Transport in superlattice direction.

The transport in direction of periodicity is the domain of genuine superlattice effects. In superlattices we are dealing with an electronic structure which differs completely from that in an uniform bulk-crystal. The band width for carriers moving in the z-direction is extremely small, typically of the order of a few meV or less, depending on the design. The energy distance between neighboring subbands is also small and can be tailored in-

dependently within wide limits (see section 2). The Brillouin zone is reduced by a large factor, given by the ratio (superlattice period) / (bulk lattice constant).

Two fundamentally different device aspects will be discussed here, which result from phenomena associated with this unique electronic structure. The first one is the ultra-fast response negative differential conductivity (NDC) which may be used for microwave generators down to very short wavelengths. The second one concerns directly the emission of microwave radiation by superlattices.

3.2.1. Ultra-fast response for negative differential conductivity (NDC)

Here we are concerned first with the original idea of Esaki et al. for NDC which stimulated those authors to investigate artificial semiconductor superlattices /I8/. Following to that we will consider some modifications. The basic idea of Esaki and Tsu, expressed in somewhat different terms, was to create improved conditions for the observation of "Bloch oscillations" of electrons in a band under the influence of a uniform electric field. Bloch oscillations represent the extreme limit of high-field transport and lead to NDC, as we will make plausible by a heuristic argument. An electron performs Bloch oscillations if it is accelerated by an electric field to the top of the band before it looses its momentum by a scattering process. It is then "Bragg-reflected" at the Brillouin zone boundary (see text-books like Ref. /I9/).

The condition for Bloch oscillations to occur is that the frequency of this oscillation

$$\omega_o = eFa/\hbar \qquad (20)$$

is larger than the inverse of the average momentum relaxation

time τ^{-1}, where F is the electric field and a the lattice period. This condition, however, cannot be fulfilled in any familiar semiconductor. An enormous improvement is expected for superlattices with narrow bands. The average collision or scattering rate τ^{-1} in a familiar semiconductor becomes very large when the electron energy exceeds the energy of a LO-phonon. If, however, the band width $2V_{c,\mu}$ (see Eq. (8)) is less than $\hbar\omega_{LO}$ the generation of LO-phonons by an electron becomes never allowed and the average scattering rate may be small at any value of momentum k_z within the mini-Brillouin zone $-\pi/d < k_z \leq \pi/d$, say $\tau^{-1} \simeq 10^{12} s^{-1}$. The second advantage of a superlattice is the increased period ($a \longrightarrow d \gg a$). Thus, the condition for Bloch oscillations

$$\omega_0 > \tau^{-1} \tag{21}$$

can be fulfilled at much lower fields. With a replaced by d we find for d = 10 nm that the condition is now met for $F > 10^4 Vcm^{-1}$ (whereas unreasonably high fields in excess of 10^6 or 10^7 Vcm^{-1} would be required in bulk semiconductors). Finally, avalanche breakdown due to impact ionization cannot occur because of the low kinetic energy of the carriers, and inter-subband tunneling (the superlattice analogue to Zener tunneling) can be made small by appropriate design of the structure.

The mechanism for NDC can be made plausible by the following semiclassical argument /20/. Assume, that the emission rate for (acoustic) phonons by electrons which pass through the Brillouin zone under the influence of the electric field F is independent of the Bloch frequency ω_0. The average energy dissipation per phonon emission process is

$$\Delta\varepsilon \simeq \hbar\bar{\omega}_{ac} \tag{22}$$

(where $\hbar\bar{\omega}_{ac}$ is the average energy of the emitted phonons)

The dissipated energy $\Delta\varepsilon$ is provided by the electric potential

$$\phi(z) = eFz \tag{23}$$

The average drift Δz of an electron per phonon emission process follows to be

$$eF\Delta z = \hbar\bar{\omega}_{ac} \tag{24}$$

and the drift velocity of the electrons is obtained by multiplying Δz with the emission rate τ^{-1}

$$v_{dr} = \Delta z\,\tau^{-1} = \hbar\bar{\omega}_{ac}/(eF\tau) \tag{25}$$

Thus, the current in the "high-field" regime becomes

$$j = env_{dr} = en\hbar\omega_{ac}/(eF\tau) \tag{26}$$

whence

$$j \propto F^{-1} \tag{27}$$

follows. Consequentely, the differential conductivity

$$\sigma_{diff} = dj/dF \propto -F^{-2} \tag{28}$$

is negative.

The most appealing property of this mechanism for NDC is the instantaneous response of the current to the extrenal field. In contrast to other processes, like NDC in the Gunn effect, there is no transient behavior expected. This is so, because no redistribution of carriers in real or momentum space has to occur before the field-dependence of j according to Eq. (26) applies. Therefore, this mechanism is suitable for very high frequency microwave generation.

The real situation, however, is somewhat different from our idealized picture:

1) The average scattering time of $\tau \simeq 10^{-12}$s assumed so far is probably shorter in real samples. $\tau = 10^{-12}$s corresponds to a (low-field) mobility of $\mu = 2.5 \times 10^4 \text{cm}^2\text{V}^{-1}\text{s}^{-1}$ in bulk GaAs. The dopants which are indispensable for providing the elctrons will allow for such high mobility only at very low carrier concentrations (note, that the advantage of modulation doping, at least, is not very effective in the case of rather narrow barriers of s.c.^{II} between the potential wells in s.c.^{I}). In addition, these scattering times apply only for a topologically nearly perfect superlattice.

2) Even with τ as large as 10^{-12}s the condition for Bloch oscillations (21) yields $eFd \simeq 10$ meV. This implies that the potential drop per superlattice period is comparable with the subband width $2V_{c,o}$ (see Eq. (8)). The (classical) amplitude of a Bloch oscillation is /20/

$$\Lambda_o = 2V_{c,0}/eF \tag{29}$$

It is clear that the description of transport in terms of Bloch oscillations breaks down if $\Lambda < d$ which is equivalent with

$$eFd > 2V_{c,o} \tag{30}$$

Fortunately, the NDC persists also in this case, as shown in Refs. /21,22/. The transport has now to be described in terms of hopping between adjacent potential wells. The qualitative dependence between drift velovity $v_{dr} = d\, w(eU_d)$ and potential drop $eU_d = eFd$ between adjacent potential wells is shown in Fig. 8. The increase of $v_{dr}(eU_d)$ for $eU_d > eU_2$ may originate from various phenomena such as from interband tunneling of electrons from the E_o- into the E_1 -band. The region of negative differential mobility

$$\mu_{diff} = d v_{dr}/d(eU/d) < 0 \; ; \; eU_I < eU_d < eU_2 \tag{31}$$

which follows the linear and sub-linear low-field region, $eU_d < eU_I$, again

is a region where the response follows the voltage instantaneously.

Stability considerations. For short times the dependence between the current density

$$j = env_{dr}(eFd) \tag{32}$$

and (average) electric field $F = U_{tot}/L_z$ has the same shape as $v_{dr}(eU_d)$ in Fig. 8 ($L_z = Nd$ is the total length of the superlattice structure). Because of the instability of the region

$$eU_1 < eU_d < eU_2 \tag{33}$$

however, we expect time-dependent effects to be important when the applied bias U_{tot} is in the range

$$NU_1 < U_{tot} < NU_2 \tag{34}$$

A stationary state is characterized by the current continuity condition

$$j_{m,m+1} = en_m^{(2)} v_{dr}(eU_{m,m+1}), \qquad \text{for all } m \tag{35}$$

where m refers to the m-th period of the superlattice..

What happens, if the total external potential exceeds

$$eU_{tot} > NeU_1 \quad ? \tag{36}$$

Naively, we expect that j decreases with increasing U_{tot} until the external potential becomes

$$eU_{tot} = (N-1)\, eU_1 + eU_3 \tag{37}$$

At this voltage the current would jump back to its maximum value

$$j^{max} = e n^{(2)} v_{dr}^{max}/d \tag{38}$$

($n^{(2)}/d$ corresponds to the 3-dimensional carrier concentration). With further increasing U_{tot} such jumps would occur each time if the condition

$$eU_{tot} = (N-m)\,eU_1 + m\,eU_2 \qquad (39)$$

is met. This interpretation was used in Ref. /21/ where oscillations of the conductivity observed in a $Al_xGa_{1-x}As$-GaAs superlattice were interpreted in these terms.

A rigorous treatment, however, has to take into account the relation between change in voltage drop between two neigboring pairs of potential wells and the carrier concentration. In Fig.9 this is illustrated. The change of potential drop between the m-th and the (m+1)-th potential well compared with the potential drop between (m-1) and m

$$\Delta eU_m = eU_{m,m+1} - eU_{m-1,m} \qquad (40)$$

is only possible with additional free carriers in the m-th well. Poisson's equation requires an additional electron concentration in the m-th layer $\Delta n_m^{(2)}$, given by

$$\Delta eU_m \simeq 4\pi e^2 \Delta n^{(2)} d/\kappa_o \qquad (41)$$

The continuity condition for the current, therefore, becomes

$$e\,n_{m-1}\,v_{dr}(eU_{m-1,m}) = e\left[n_o^{(2)} + \frac{\Delta eU_m \kappa_o}{4\pi e^2 d}\right] v_{dr}(eU_{m-1,m} + \Delta eU_m) \qquad (42)$$

For a reasonable value of $\Delta eU_m \simeq 50meV$ and $d = 10nm$ we obtain $\Delta n^{(2)} \simeq 3.5\times10^{11}cm^{-2}$ from Eq. (41). From Eq. (42) we now see that $j_{m,m+1}$ no longer contains necessarily a range of NDC for $eU_{m-1,m} > eU_1$. The answer to the question whether it does or not, depends on the shape of $v_{dr}(eU_d)$ and on the value of carriers per layer in the neutral bulk superlattice $n_o^{(2)}$: If $n_o^{(2)}$ is small, the relative increase of carrier concentration due to $\Delta n^{(2)}(\Delta eU_m)$ is everywhere large enough to overcome the decrease of v_{dr} in Eq. (42). Thus, oscillations of current as a function of applied total voltage, $j(U_{tot})$, will occur only in samples with sufficiently high carrier concentration in the ground state and with large negative slope of the v_{dr} vs. eU_d curve. The behavior according to Eq. (39) occurs in the limiting

case of very large $n_o^{(2)}$ and/or steep increase of $v_{dr}(eU_d)$ in the range $eU_1 < eU_d < eU_2$. More important is the time scale for establishing a steady state situation. It can by estimated by the time required to accumulate a charge of the order of $\Delta n^{(2)}(eU_{m,m+1})$ due to the difference between the currents

$$\Delta j_m = j_{m,m+1} - j_{m-1,m} \tag{43}$$

With $j_{m,m+1} \simeq 0.5\ j_{m-1,m}$ we find

$$0.5\ n_o^{(2)} w^{max} t = \Delta n^{(2)} \tag{44}$$

$$t = (w^{max})^{-1} \frac{\Delta n^{(2)}}{n_o^{(2)}} \tag{45}$$

The maximum value of the interlayer transition probability is determined by the design parameters. It should not excced a value of $^{max} \simeq 10^{12} s^{-1}$ in order to guarantee energy relaxation of the carriers before hopping to the next potential well. It should be noted, that $w^{max} \simeq 10^{12} s^{-1}$ is probably prohibited also by the high power dissipation associated with $w^{max} \simeq 10^{12} s^{-1}$ and $n_o^{(2)} \simeq 10^{12} cm^{-2}$ because it implies a very high current density of $j \simeq e w^{max} n_o^{(2)} \simeq 1.6 \times 10^5 Acm^{-2}$. If, however, w^{max} is chosen by orders of magnitude smaller the response time for steady state becomes rather long according to Eq. (45).

Before we conclude this section we would like to discuss briefly the idea of NDC in a <u>double barrier</u> system which was originally proposed by Esaki et al. / 22, 23 /. We will, however, include the space charge effects into our consideration. It turns out that the space-charge effects in this device can either be eliminated or be used favorably, depending on design and on intension.

In contrast to Esaki et al. we consider the transport across the double barrier as a two-step process, characterized by

transition probabilities $w_{lm}(V_{lm})$ and $w_{mr}(V_{mr})$. This is, at least, the more appropriate description if

$$(w_{lm}, w_{mr}) < \tau_m^{-1},$$

where τ_m is the relaxation time of carriers in the central layer. The transition probability $w_{lm}(V_{lm})$ reflects the resonances for $V_{lm} = E_o, E_1, \ldots$, whereas $w_{mr}(V_{mr})$ for carriers in the E_o subband is rather structureless for $V_{mr} > E_o$.

Case 1: w_{mr} is assumed to be significantly larger than for any potential drop of interest. There are no carriers in the central layer at zero external bias, nor is there an appreciable carrier accumulation in that layer under external bias. The transport through the double barrier is mainly determined by the product of the probability $w_{lm}(V_{lm})$ and the (nearly constant) carrier concentration in the electron accumulation layer between $GaAs_1$ and $Al_xGa_{1-x}As_1$. Therefore the current-voltage characteristic is stable in the region where $dw_{lm}/dV_{lm} < 0$ and its shape does not differ significantly from Fig. ; only the voltage scale is expanded by a factor of about two. The response to the applied voltage is quasi-instantaneous.

Case 2: A rather large carrier concentration is present in the m-layer at zero voltage (or, in other words: E_o-states are populated in the ground state when the Fermi levels ϕ_l, ϕ_m, and ϕ_r coincide). In Fig. II w_{lm} and w_{mr} are shown as a function of $eU_{lm} = \phi_l - \phi_m$ and $eU_{mr} = \phi_m - \phi_r$, respectively. For convenience we assume equal carrier concentration in the accumulation layer, $n_{l,o}^{(2)}$ and in the middle layer, $n_{m,o}^{(2)}$, at zero bias. Furthermore, we assume $\phi_l - \phi_m \simeq \phi_m - \phi_r \simeq (\phi_l - \phi_r)/2 \simeq eU_{tot}/2$ after turning on the external bias U_{tot}. In the range $2\phi_1 < eU_{tot} < 2\phi_2$ we have

$$j_{lm}(t \gtrsim 0) < j_{mr}(t \gtrsim 0) \Rightarrow \frac{dn_m^{(2)}}{dt} < 0 \Rightarrow \frac{d(\phi_l - \phi_m)}{dt} > 0 \quad (46)$$

A bistable steady state current situation $j_{lm}(t\to\infty) = j_{mr}(t\to\infty)$ as a function of eU_{tot}, similar to the case discussed for doping superlattices in Ref. /23/, section 5.1.3 is obtained for this case.

3.2.2. Spontaneous and stimulated FIR emission from interlayer transitions.

There is a large number of mechanisms for transitions of charge carriers between adjacent layers of a superlattice. In the following we will be concerned with radiative interlayer transitions under the influence of an electric field. In this report we will restrict ourselves to the consideration of radiative transitions within the lowest subband (no intersubband transitions!). Non-radiating interlayer transitions in a superlattice due to electron-phonon and electron-impurity scattering have been calculated in Ref. /20/. It was found that the probability for these processes contains a reduction factor $(V_{c,o}/eFd)^2$ compared with corresponding bulk values, if the potential drop per superlattice period eFd is large compared with the mini-band width $2V_{c,o}$. For the calculation of radiative interlayer transitions the results of an exact calculation in the one-band approximation /25/ can be applied to our specific case. The result from Ref. /25/ reads for transitions within a thight binding band in terms of our superlattice parameters

$$w^{rad}(\hbar\omega) = \frac{4e^2}{3c^3\hbar^4}\, eFd\, d^2\, |V_{c,o}|^2\, \delta(\hbar\omega - eFd) \qquad (47)$$

For $d = 20$ nm, $V_{c,o} = 1$ meV, $eFd = 10$ meV the rate of emission of photons with $\hbar\omega = 10$ meV per electron becomes

$$w^{rad} \simeq 2.5\times 10^3\ s^{-1} \qquad (48)$$

The efficiency η, i.e. the ratio betwee radiative and non-radiative transitions if more favorable than in the case of FIR radiation from transport parallel to the layers (see section 3.1.3)

for two reasons:

1) No LO-phonons will be emitted, unless eFd exceeds the value of $\hbar\omega_{LO}$

2) The probability for non-radiative interlayer transitions by the emission of acoustic phonons is reduced by the factor $(V_{c,o}/eFd)^2$ compared with a uniform bulk material, as shown in Ref. /20/. This means a net increase of efficiency by a factor of 10^2 for our example.

There is, however, a problem which originates from the translational symmetry of the superlattice in z-direction. For illustration we consider the Fig. I2 . For a calculation of the emission rate in a system with $n^{(2)}$ electrons per layer the population factors $f(\mathcal{E}_o(\vec{k}_\parallel))$ have to be included. For spontaneous transitions from the m-th into th (m+1)-th layer we obtain

$$\dot{n}^{(2)\,sp.}_{m\to m+1} = \frac{2}{4\pi^2}\int d^2k_\parallel w_{m\to m+1} f^{(m)}(\mathcal{E}_{k_\parallel})\left(1-f^{(m+1)}(\mathcal{E}_{k_\parallel})\right) \qquad (49)$$

The distribution functions $f^m(\mathcal{E}_{k_\parallel})$ in Eq. (49) do not depend on the layer index, because of the translational symmetry of the system. They are given by the Fermi-function for a two-dimensional system of $n^{(2)}$ electrons

$$f(\mathcal{E}_{k_\parallel}) = \left\{\exp\left[\hbar^2(k_\parallel^2 - 2\pi n^{(2)})/2m_c kT_e\right] + 1\right\}^{-1} \qquad (50)$$

T_e is the electron temperature, which may be larger than the lattice temperature. Integration in Eq. (49) yields

$$\dot{n}^{(2)\,sp.}_{m\to m+1} \simeq N^{(2)} kT\, w_{m\to m+1} \qquad (51)$$

if the Fermi energy $(\hbar^2/2m_c)(2\pi n^{(2)})$ is comparable with kT or larger ($N^{(2)} = m_c/(\pi\hbar^2)$ is the two-dimensional density of states). Note, that increasing values of $n^{(2)}$ <u>will not</u> increase the intensity of spontaneous radiating interlayer transitions, but will only increase the non-ratiating processes!

A very important consequence of the translational symmetry

is its effect on absorption and stimulated emission in the superlattice: Whatever the temperature is, the stimulated emission processes ($m \rightarrow m+1$) will be exactly compensated by absorption processes ($m \rightarrow m-1$). Therefore, there will be no gain in this system.

We will now show, how this fediciency can be overcome by replacing the ordinary superlattice by a"superlattice with superstructure" of appropriate design (Fig. I3a). The barrier widths d_a^{II} and d_b^{II} are chosen sufficiently thick in order to guarantee that the carriers will thermalize after each interlayer transition within the potential wells of width d_a^I and d_b^I before making further transitions into the adjacent potential well. Moreover, the (b)-barriers are thinner than the (a)-barriers. Thus, the steady state electron concentration $n_b^{(2)}$ in the (b)-wells will be smaller than $n_a^{(2)}$, because of the higher transition probabilities through the former ones **(Figs. I3 b and c)**

It is now evident from Fig. that we have now pupulation inversion for the ($a \rightarrow b$)-transitions with $k_{\parallel}$-conservation within the range of momentum values

$$k_{F,b} < |\vec{k}_{\parallel}| < k_{F,a} \qquad (52)$$

with $k_{F,b} = (2\pi n_b^{(2)\,st})^{1/2}$ and $k_{F,a} = (2\pi n_a^{(2)\,st})^{1/2}$, where $n_b^{(2),st}$ and $n_a^{(2),st}$ are the steady state carrier concentrations under a given external bias in the (b)- and (a)-layers, respectively.

The energy of the FIR radiation is tunable by variation of the applied bias. At large concentrations of $n^{(2)} = n_a^{(2)} + n_b^{(2)}$ space charge effects have also to be taken into account, just as in the cases discussed in section 3.2.1.

The gain for photons with polarization in z-direction is given by

$$g(\hbar\omega) \simeq (4\pi e^2\omega/n_r c)\, d^{-1} \sum_{\vec{k}_\parallel} |\langle a,\vec{k}_\parallel|z|b,\vec{k}_\parallel\rangle|^2 \cdot f^{(a)}(\hbar^2(k_\parallel^2 - k_{F,a}^2)/2m_e)\left[1 - f^{(b)}(\hbar^2(k_\parallel^2 - k_{F,b}^2)/2m_e)\right] \cdot \delta(\hbar\omega - (E^a - E^b)_F) \quad (54)$$

($(E^a - E^b)_F$ is the steady state energy difference under the given external bias).

In real systems the gain depends on how much the δ-function in Eq. (54) will be broadened. Assuming a width of 1 meV, d = 10 nm, eFd = $\hbar\omega$ = 10 meV, $V_{c,o}$ = 1 meV, $n_a^{(2)} - n_b^{(2)} = 10^{11}\,cm^{-2}$, and for the real part of the refractive index n_r = 3.5 we find

$$g(10meV) \simeq 300\ cm^{-1} \quad (56)$$

From this estimate it follows that a sufficiently high gain for the construction of a FIR laser could be achieved, even if the estimates given above might be somewhat too optimistic.

4. Properties, specific for doping superlattices

The specific properties, which make doping superlattices suitable for a large number of novel devices are the tunability of effective band gap and carrier concentration and the extremely long lifetimes which can be achieved.

Most of the device aspects associated with these properties have been discussed in a chapter for the book "The Technology and Physics of Molecular Beam Epitaxy" /26/ (a copy of the manuscript is attached to this report). In the present report we will only tie together the essential findings of that document.

Table 1 gives an overview about some of the properties (conductivity, optical absorption, stimulated and spontaneous light emission) which can be modulated by external bias and/or light. A few "electro-electrical", electro-optical, opto-electric, and "opto-optical" devices are listed at the appropriate locations in this matrix. This list corresponds to those devices discussed in Ref. 26.

We want to point out the following facts:

1) The large variety of n-i-p-i devices results from the possibility to vary many properties by different means (see Table 1). The first two options, modulation by light and by external bias U_{np}, are qualitatively similar in some respect: In both cases the carrier concentration is changed. In the case of electric modulation the carriers are injected (or extracted) through selective n- and p-electrodes. Optic modulation is achieved by electron-hole pair generation and subsequent spatial separation due to the internal space-charge fields. The modulation, in both cases implies a constant, but different quasi Fermi level for electrons, ϕ_n, and holes, ϕ_p, throughout the crystal (see Fig.s 3 and 4). The speed of these devices is, therefore, determined by the time within which these changes can be achieved.

The responsetime on an optical signal may be very short. The decay time for this response, i.e. the recovery time, is limited by the lifetime of the carriers. Therefore, it can be extremely long, but also rather short, depending on the design parameters of the n-i-p-i structure (the range from ks to ns, i.e. 12 orders of magnitude is readily achievable). Thus, a high sensitivity photodetector, which is based on the long lifetimes of the photoconductive response, will show a very long recovery time. (This is true only for the simplest version; see, however, p.41 of Ref.26 (Section 5.1.1.2.3))

The speed for variation by the external potential eU_{np} depends on the time constant $\tau_{np} = R_{np}C_{np}$ of the device. Here, R_{np} is the series resistance of the n- and p-layers, and C_{np} is the capacitance of the n-i-p-i structure associated with changes of the carrier concentration $n^{(2)}$ and $p^{(2)}$ in the layers and the change of the effective band-gap $E_g^{eff,n}$ ($\simeq \phi_n - \phi_p$). This time constant τ_{np} depends quadratically on the lateral dimensions (L_x and/or L_y) of the device and also on the electron and hole mobilities.

The third possibility of varying the electronic structure, the modulation by an external field F_z in direction of periodicity (see Fig.14), can be achieved by the application of an external voltage U_z via sandwich electrodes. This procedure differs in two important points from the modulation by light or by the voltage U_{np} : i) This modulation implies both, an increase (with respect to the neighboring n-layer to the left in Fig.14) and a decrease (with respect to the neighboring n-layer to the right in Fig.14) of the effective band-gap. ii)This modulation is not associated with a change of carrier concentration in the n-i-p-i structure. Therefore, the speed of modulation is only limited by the time-constant for a modulation of the voltage U_z. This time constant $\tau_z = R_zC_z$ is the product of the (rather small)

capacitance of the n-i-p-i structure of total thickness L_z (and not of the superlattice period d !) and the electrode resistance, R_z, which can be very small for sandwich electrodes applied to a n-i-p-i structure on a n^+- substrate and with a n^+ top layer.

The modulation by this kind of electrodes implies the possibility for ultra-fast modulation of the conductivity in z-direction (including the range of negative differential conductivity in n-i-p-i semimetals). The most important application, however, will probably be found in the field of optoelectronics, since ultrafast modulators (based on the variation of absorption for photon energies $\hbar\omega < E_g^o$) and ultra-fast tunable light sources (LED's and lasers) can be made from n-i-p-i crystals. (so far, only the theoretical concept exists, but there are no principal problems to be expected).

2) The variety of devices and the range of their possible applications becomes particularly wide by the enormous flexibility in designing n-i-p-i structures for particular purposes. This flexibility includes, apart from the choice of doping concentrations and layer thicknesses, also the choice of the host material. Note, that any semiconductor can be chosen as the host for a n-i-p-i structure, provided there is a growth technique available which allows for periodic modulation of n- and p-doping. If, in addition, the host material can be lattice-matched with another one, the growth of hetero n-i-p-i crystals becomes feasible (see Fig.4). The most important properties by which these superlattices differ from ordinary n-i-p-i structures, are high electron and hole mobilities and narrow luminescence lines /11,13,27,28/. In this way many properties can be optimized simultaneously with respect to very different parameters of a given device. Thus, e.g., the high sensitivity of a photodetector for a given long wavelength photon energy can coexist with low dark currents and low noise level.

References.

1) See, for instance, Proceedings of the Conference on Metastable Modulated Semiconductor Structures, J. Vac. Sci. Technol. B1 (1983), and Proceedings of the Int. Conferences on the Electronic Properties of 2-dimensional Systems, Surface Science 58 (1976), 73 (1978), 98 (1980) and 113 (1982)

2) H.L.Stoermer, A.Pinczuk, A.C. Gossard, and W. Wiegmann, Appl. Phys. Lett. 38, 681 (1981).

3) K. von Klitzing, G. Dorda, and M. Pepper Phys. Rev. Lett. 45, 494 (1980).

4) G.H. Doehler, phys. stat. sol. (b) 52, 79 and 533 (1972).

5) G.H. Doehler, H. Kuenzel, D. Olego, K. Ploog, P. Ruden, H.J.Stolz, and G.Abstreiter, Phys. Rev. Lett. 47, 864 (1981)

6) G.H. Doehler, Japan. J. of Appl. Phys. 22, Suppl. 22-1, 29 (1983)

7) G.H. Doehler, in "Festkoerperprobleme: Advances in Solid State Physics", edited by P. Grosse (Vieweg, Braunschweig, 1983), Vol. XXIII, p. 207

8) T. Mimura, S. Hiyamizu, T. Fujii, an K. Nabu, Japan. J. Appl. Phys. 19, L225 (1980)

9) S. Hiyamizu, in "Collected Papers of 2nd Int. Symp. on Molecular Beam Epitaxy and Related Clean Surface Techniques", R. Ueda, Ed. (Tokyo, 1982), p. 113

10) D. Delagebeaudeuf, P. Delescluse, P. Etienne, M. Laviron, J. Chaplart, and N.T. Linh, Electr. Lett. 16, 667 (1980)

11) G.H. Doehler, Physica Scripta 24, 430 (1981)

12) K. Ploog and G.H. Doehler, Advances in Physics 32, 258 (1983)

13) H. Kuenzel, A. Fischer, J. Knecht, and K. Ploog, Appl. Phys. A 30, 73 (1983)

14) M. Inoue, S. Hiyamizu, M. Inayama, and Y. Inuishi, Japan. J. Appl. Phys. 22, Suppl. 22-1, 357 (1983)

15) K. Hess, H. Morkoc, H. Shichjo, and G.B. Streetman, Appl. Phys. Lett. 38, 469 (1979)

16) M.A. Littlejohn, W.M. Kwapien, T.H. Glisson, and J.R. Hauser, J. Vac. Sci. Technol. B 1, 445 (1983)

17) E. Gornic and D.C. Tsui, Phys. Rev. Lett. 37, 1475 (1976) and E. Gornic, R. Schwarz, G. Lindemann, and D.C. Tsui, Surface Sci. 98, 493 (1980)

18) L. Esaki and R. Tsu, IBM J. Res. Dev. 14, 61 (1970)

19) J.M. Ziman, Principles of the Theory of Solids (Cambridge, 1965), p. 164

20) G.H. Doehler, R. Tsu, and L. Esaki, Solid State Commun. 17, 317 (1975)

21) L. Esaki and L.L. Chang, Phys. Rev. Lett. 33, 495 (1974)

22) L.L. Chang, L. Esaki, and R. Tsu, Appl. Rev. Lett. 24., 593 (1974)

23) L. Esaki and L.L. Chang, Thin Solid Films 36, 285 (1976)

24) G.H. Doehler in "Collected Papers of 2nd Int. Symp. on Molecular Beam Epitaxy and Related Clean Surface Techniques", R. Ueda, Ed. (Tokyo, 1982), p. 20

25) G.H. Doehler, and K. Hacker, phys. stat. sol. 26, 551 (1968)

26) G.H. Doehler in "The Technology and Physics of Molecular Beam Epitaxy", E.H.C. Parker and M.G. Dowsett, Eds. (Plenum, N.Y., 1984), to be publ.

27) P. Ruden and G. Doehler, J. Vac. Sci. Technol., to be published

28) G.H. Doehler and P. Ruden, Surface Science, in press

Fig.1

Heavy lines: Superlattice potential resulting from the periodic variation of the conduction and valence band edges, in a type-I compositional superlattice. The edges of the two lowest conduction and uppermost valence subbands are shown together with the lowest subband wave functions $\Psi_{c,0}(z)$ and $\Psi_{v,0}(z)$, respectively, by light lines.

Fig.2

Same, as in Fig.1, but for type-II compositional superlattice.

Fig.3

Superlattice potential in a doping superlattice (n-i-p-i crystal) resulting from the periodic modulation of the conduction and valence band edges, $\mathcal{E}_c(z)$ and $\mathcal{E}_v(z)$ by the impurity space charge potential. The numbers o, 1, 2,... label the subband edges. For the 0-th subbands the wave functions are indicated. (a) ground state, without free carriers in the doping layers. (b) excited state with electrons and holes in the n- and p-layers, with increased band gap ($E_g^{eff,o} \longrightarrow E_g^{eff,n}$) and different quasi Fermi levels ϕ_n and ϕ_p for electrons and holes. The hatched areas indicate the tunneling barriers for electron-hole recombination processes.

Fig.4

Same as in Fig.3, however for a hetero-doping superlattice. In this system the n- and p-doping is confined to the larger band gap material, s.c.^{II} and the carriers are confined to the smaller band gap material, s.c.^{I} . Electrons and holes are spatially separated, as in familiar n-i-p-i crystals. In addition, they are spatially separated from their parent impurities, which yields high electron and hole mobilities.

Fig.5

Modulation-doped compositional superlattice. The charge carriers in the lower band gap material (GaAs) are provided by the donors in the larger band gap material ($Al_x Ga_{1-x} As$) layers, confined to a range $d_n < d^{II}$. The spatial separation between electrons and impurity atoms results in extremely weak impurity scattering and, therefore, very high low- and medium-temperature mobilities.

Fig.6

Compositional superlattice with superstructure. The layers of larger band gap material of thickness $\tilde{d}^{II}$, dividing the lower band gap layers into two layers of thickness $d^I/2$ (part b) change the subband distances strongly, depending on the value of $\tilde{d}^{II}$.

Fig.7

Schematic diagram showing the subband edges for a compositional superlattice with superstructure as shown in Fig.6 as a function of layer thickness $\tilde{d}^{II}$ with d^I kept constant (and d^{II} assumed rather large, such, that the band width with respect to the k_z -motion is negligible).

Fig.8

Relation between drift velocity, v_{dr}, and potential drop per superlattice period, $eUd = eFd$, in a superlattice with electric field F normal to the layers (schematically). For $U_1 < U_d < U_2$ the differential mobility $\mu_d = dv_{dr}/dF$ is negligible.

Fig.9

Superlattice with increased potential drop between potential wells m, and m+1. The increase of potential drop, eU_m, according to Poisson's equation , is assoziated with an increased carrier concentration, $n^{(2)}$ in the m-th potential well.

Fig.10

Double barrier structure without doping in the larger-bandgap layers and in the central lower-bandgap layer (see text, case 1). (a) Real space energy diagram with (full lines) and without (dashed lines) applied external potential eU. ϕ_l and ϕ_r indicate the Fermi levels on the left and the right, respectively. (b) Probabilities versus potential drop for transitions of a carrier on the left side to the middle layer, $w_{-1,m}$, and for a carrier in the middle layer to the right side, $w_{m,r}$, schematically.

Fig.11

Double barrier structure as in Fig.10, however with doping and with reduced tran sition probabilities $w_{m,r}$, compared with $w_{1,m}$ (see text, case 2).

Fig.12.

Real space and momentum space energy diagram of a superlattice with electric field F applied perpendicular to the layers. The momentum space picture illustrates, that transitions with $\vec{k}_{\parallel}$ -conservation are possible only near k_F and at finite electron temperatures T_e.

Fig.13

Real space, (a) and (b), and momentum space, (c), diagram of a superlattice with superstructure for the generation of microwaves by stimulated emission. The design parameters are chosen such, that inversion population takes place between the lowest subbands in type (a) and type (b) wells. The microwave frequency can be tuned by changing the field F.

Fig.14

Modulation of the electronic structure of a n-i-p-i crystal by an electric field F_z normal to the layers. For a given p-layer the effective band-gap is increased by the amount of $eF_z d/2$ with respect to the neighboring n-layer to the left and decreased by the same amount with respect to the neigboring n-layer to the right.

Table I

BY VARIATION OF:		MODULATION OF:						
		CONDUCTIVITY			ABSORPTION	GAIN	LUMINESCENCE	
LIGHT INTENSITY	EXTERNAL BIAS	σ_{nn}, σ_{pp}	σ_{np}, U_{np}	σ_z				
	1) U_{np}							
	2) U_z							
sensitive photodetectors	3-D bipol. JFET			NDC	light modulators	tunable lasers	tunable LED's	
fast photodetectors								
fast photocathodes								
high-efficiency solar cells								
ultrafast photodetector								
photo transistor								
optical light modulators	modulators							ultrafast modulated LED's
non-linear optical devices								
optically pumped	injection lasers							
optically pumped LED's	(injection)-LED's							
						ultrafast modulated		

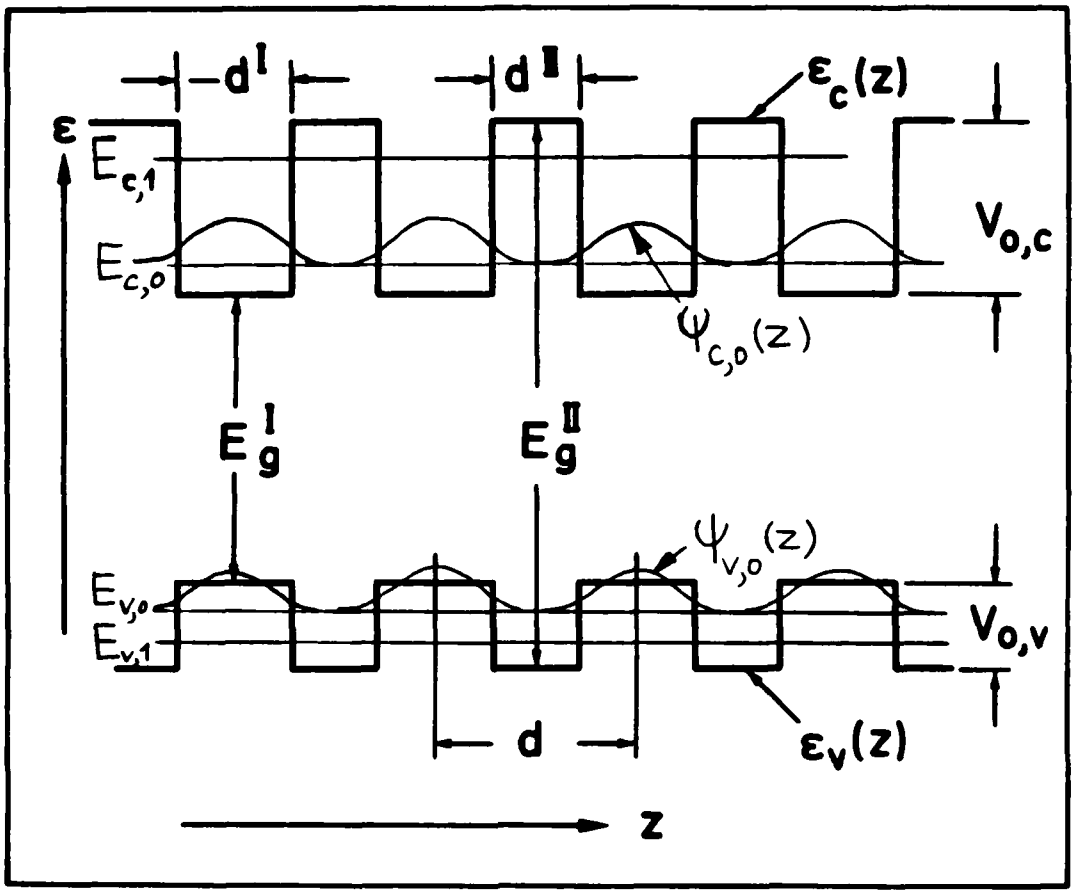
d^I
d^{II}
$\varepsilon_c(z)$
ε
$E_{c,1}$
$E_{c,o}$
$V_{o,c}$
$\Psi_{c,o}(z)$
E_g^I
E_g^{II}
$\Psi_{v,o}(z)$
$E_{v,o}$
$E_{v,1}$
$V_{o,v}$
d
$\varepsilon_v(z)$
z

Fig.

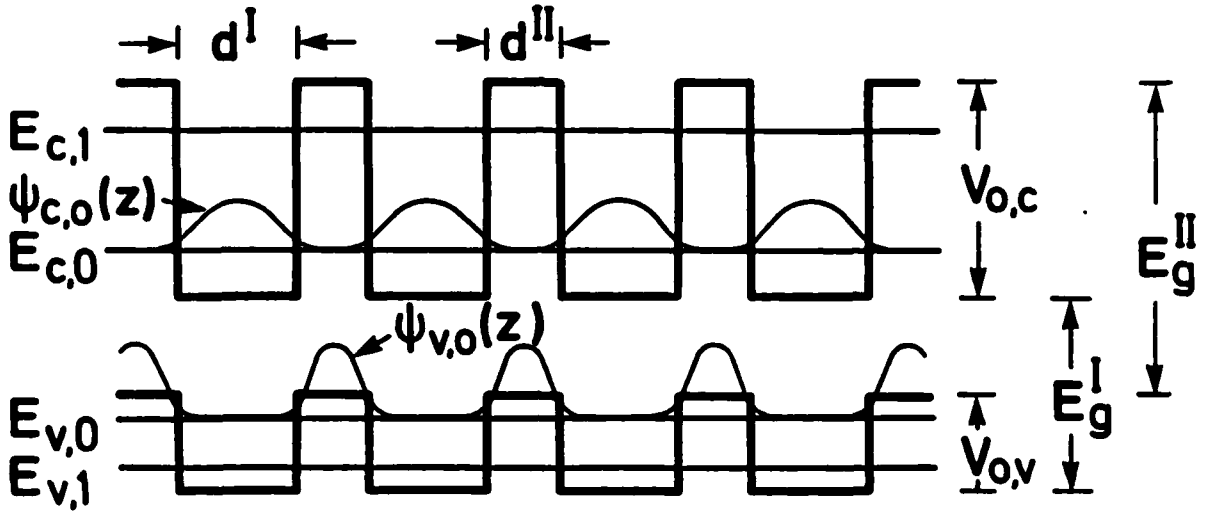
d^I
d^{II}
$E_{c,1}$
$\psi_{c,o}(z)$
$E_{c,0}$
$V_{o,c}$
E_g^{II}
$\psi_{v,o}(z)$
$E_{v,0}$
$E_{v,1}$
$V_{o,v}$
E_g^I

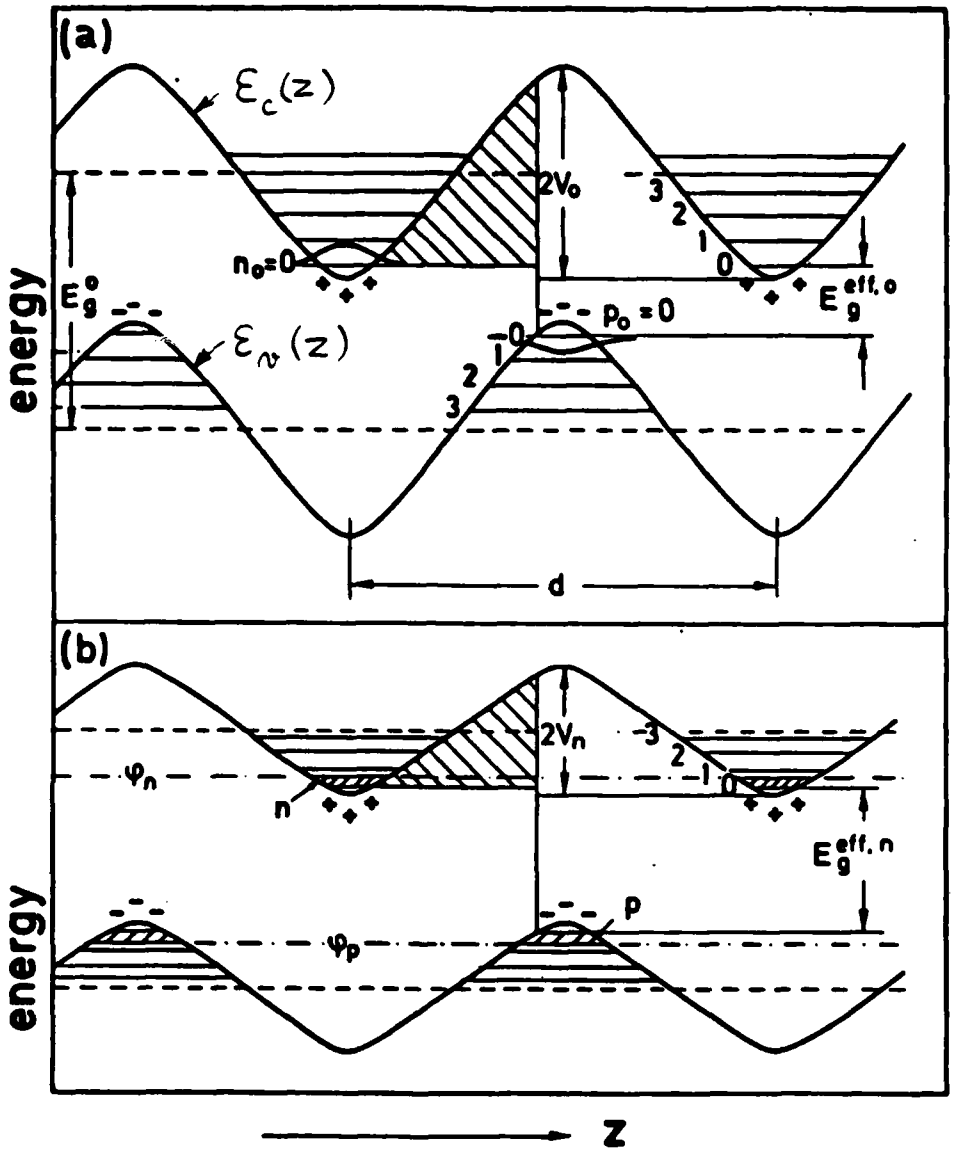
(a)
$\mathcal{E}_c(z)$
$2V_o$
3
2
1
0
$n_o=0$
E_g^o
energy
$E_g^{eff.o}$
$p_o=0$
$\mathcal{E}_v(z)$
0
1
2
3
d
(b)
$2V_n$
3
2
1
0
φ_n
n
$E_g^{eff.n}$
energy
p
φ_p
z
DIRECTION OF PERIODICITY

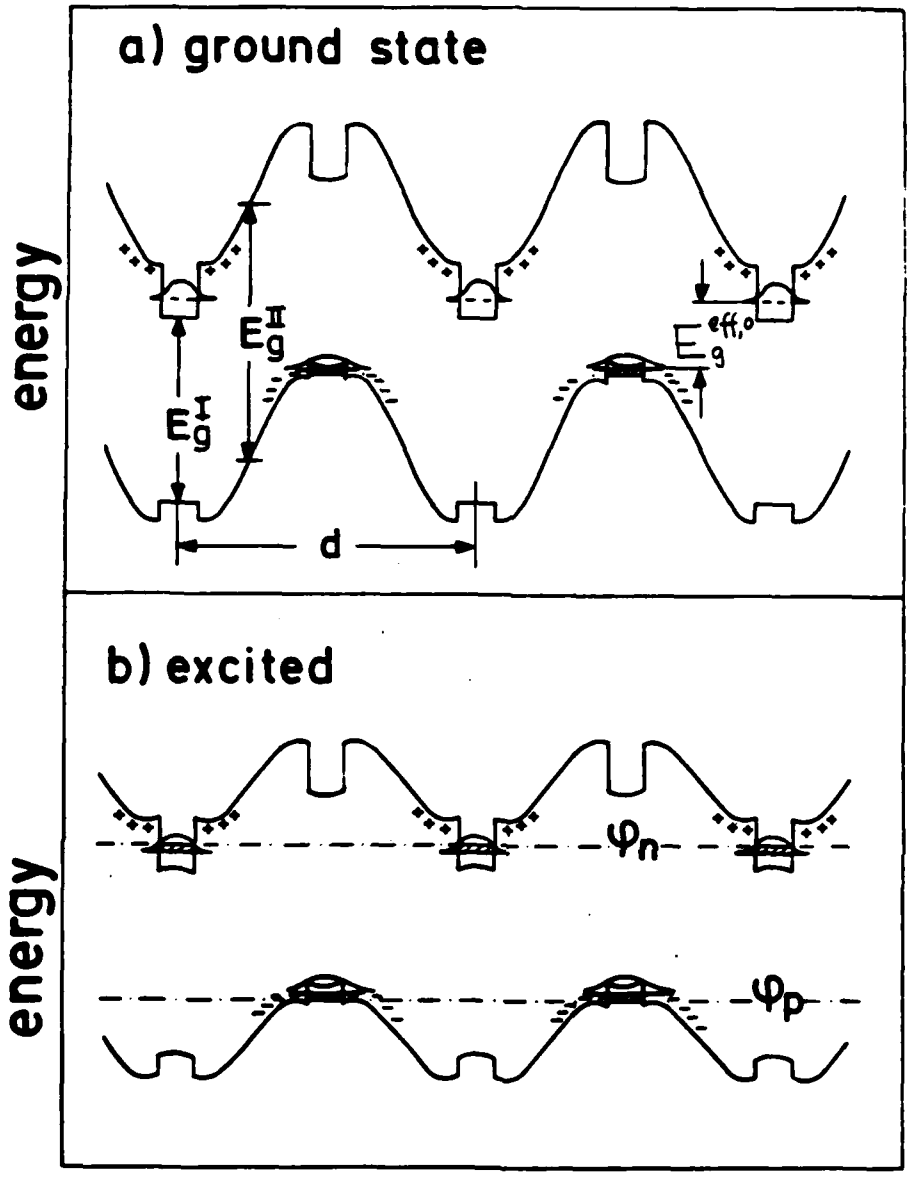
a) ground state
energy
E_g^{II}
E_g^{I}
$E_g^{eff,o}$
d
b) excited
energy
φ_n
φ_p
direction of crystal growth

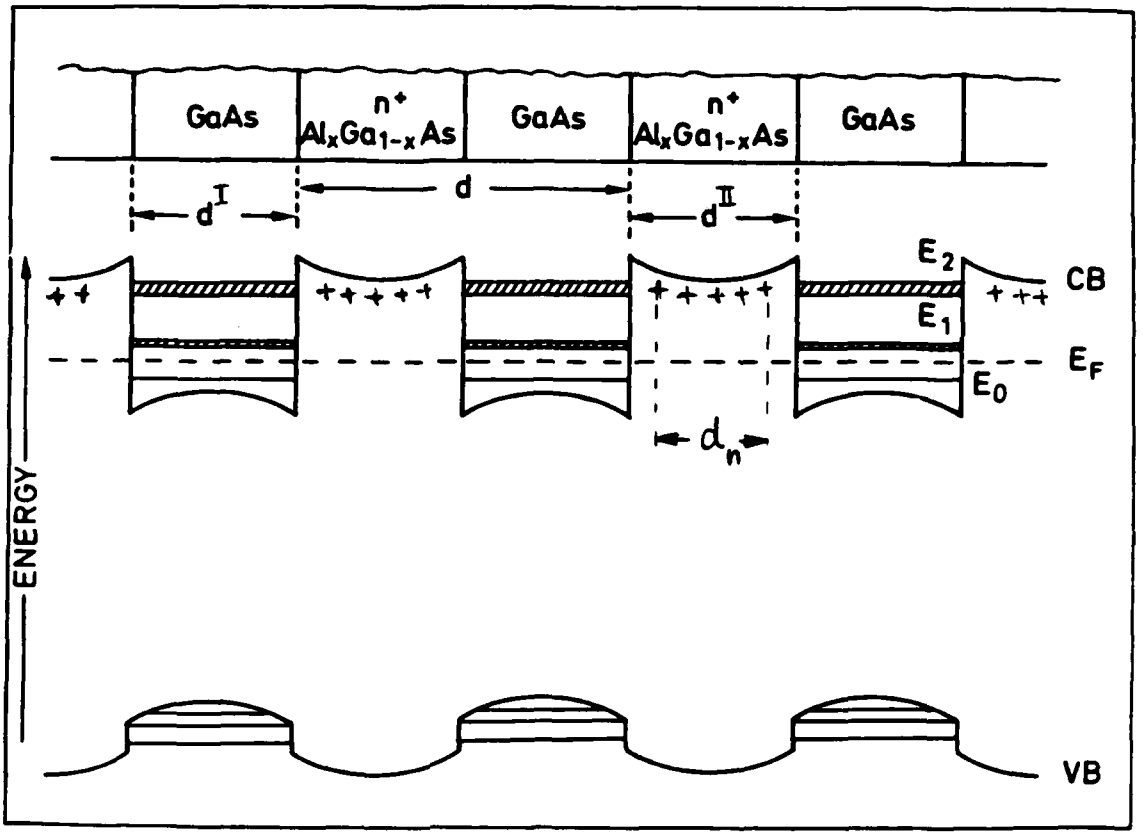
GaAs
n+
AlxGa1-xAs
GaAs
n+
AlxGa1-xAs
GaAs
d^I
d
d^II
E2
E1
E0
EF
CB
VB
dn
ENERGY
LAYER SEQUENCE

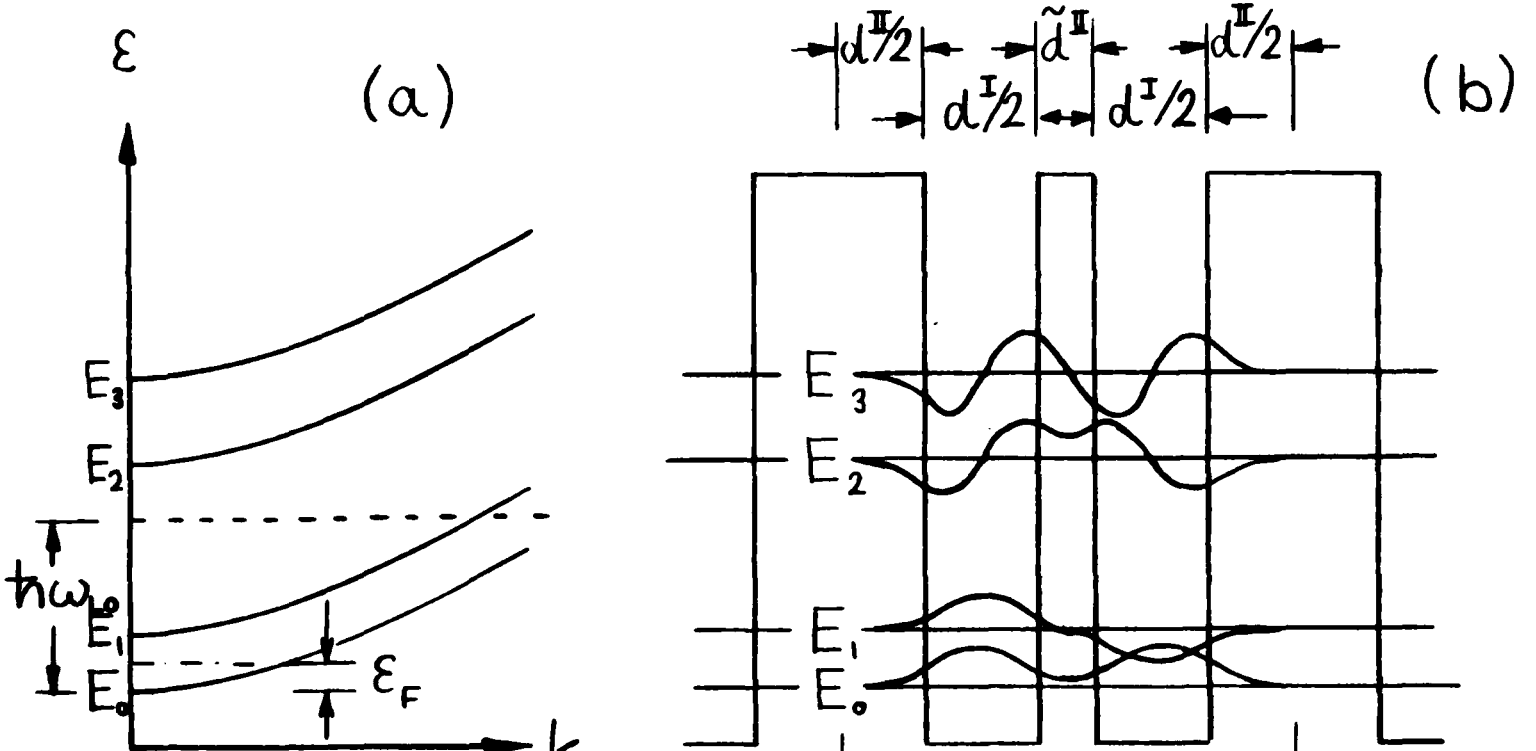
ε
(a)
E3
E2
ħω0
E1
E0
εF
k||
d^II/2
d^I/2
d̃^II
d^I/2
d^II/2
(b)
E3
E2
E1
E0
d

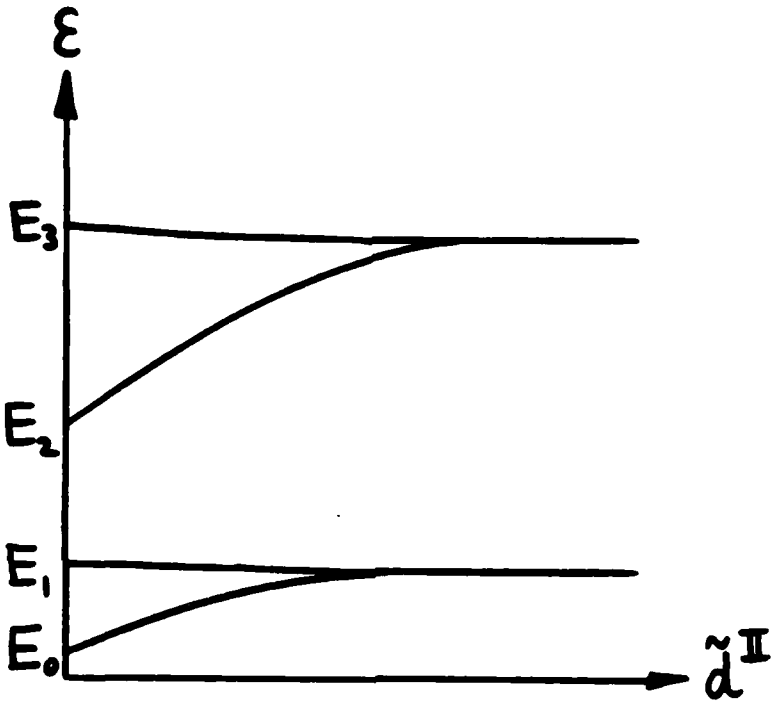

Fig. 7

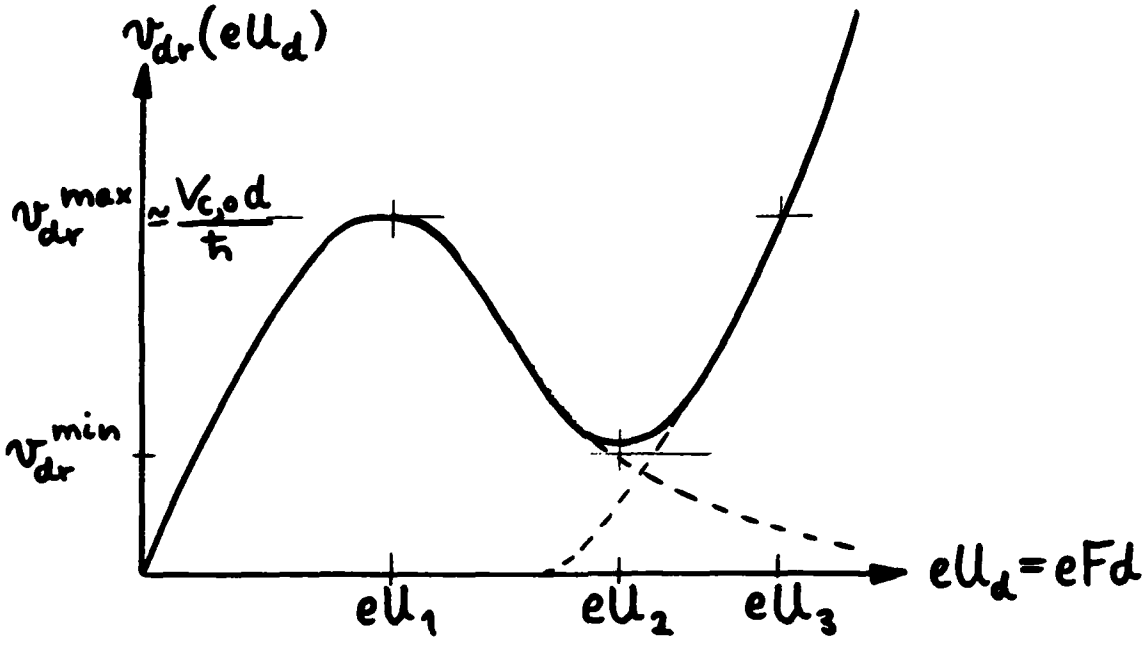
$v_{dr}(eU_d)$
$v_{dr}^{max} \simeq \frac{V_{c,0}d}{\hbar}$
v_{dr}^{min}
eU_1
eU_2
eU_3
$eU_d = eFd$

Fig. 5

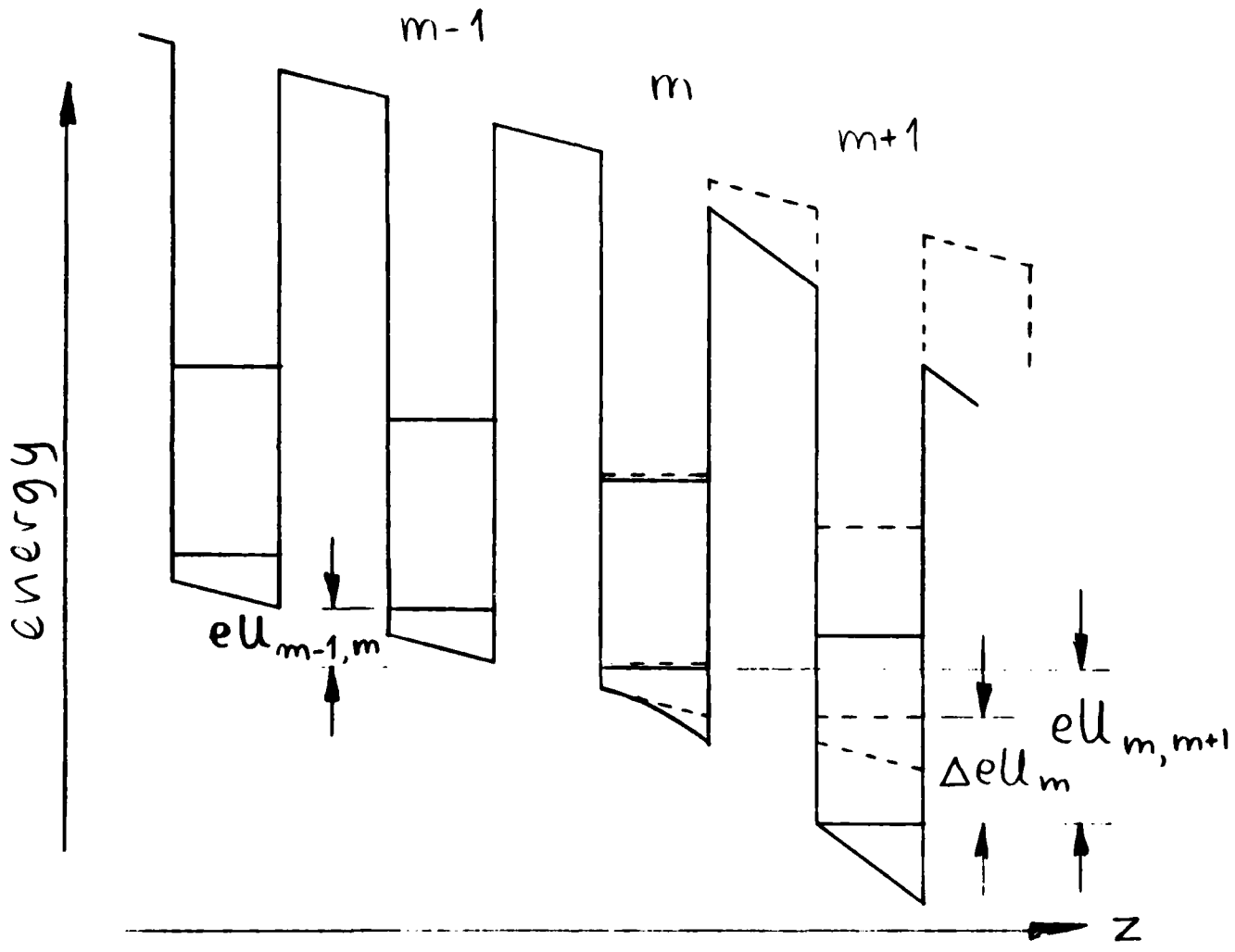
m-1
m
m+1
energy
$eU_{m-1,m}$
$eU_{m,m+1}$
ΔeU_m
z

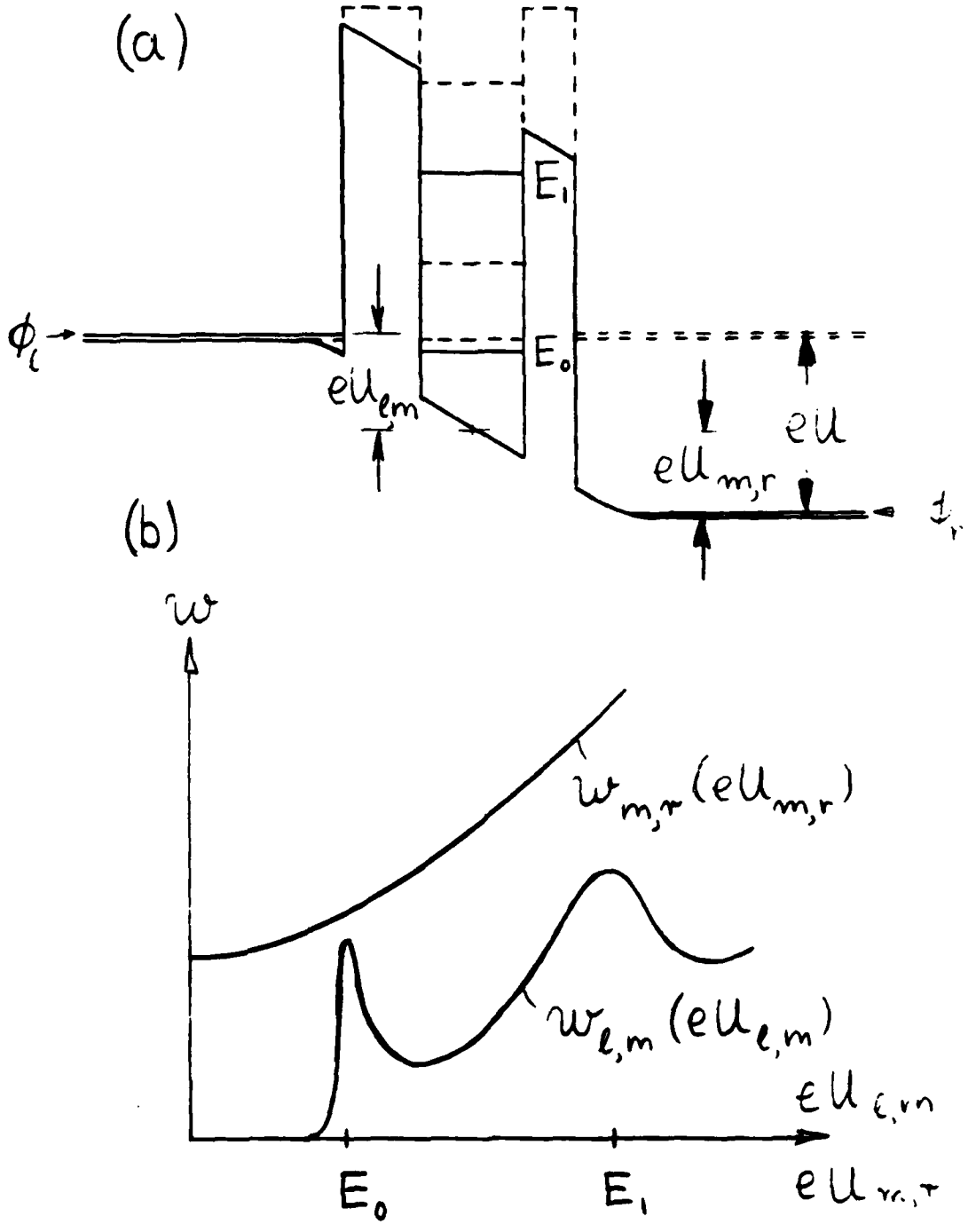
(a)
E_1
E_0
ϕ_i
$eU_{i,m}$
eU
$eU_{m,r}$
ϕ_r
(b)
w
$w_{m,r}(eU_{m,r})$
$w_{i,m}(eU_{i,m})$
$eU_{i,m}$
E_0
E_1
$eU_{m,r}$

Fig 1)

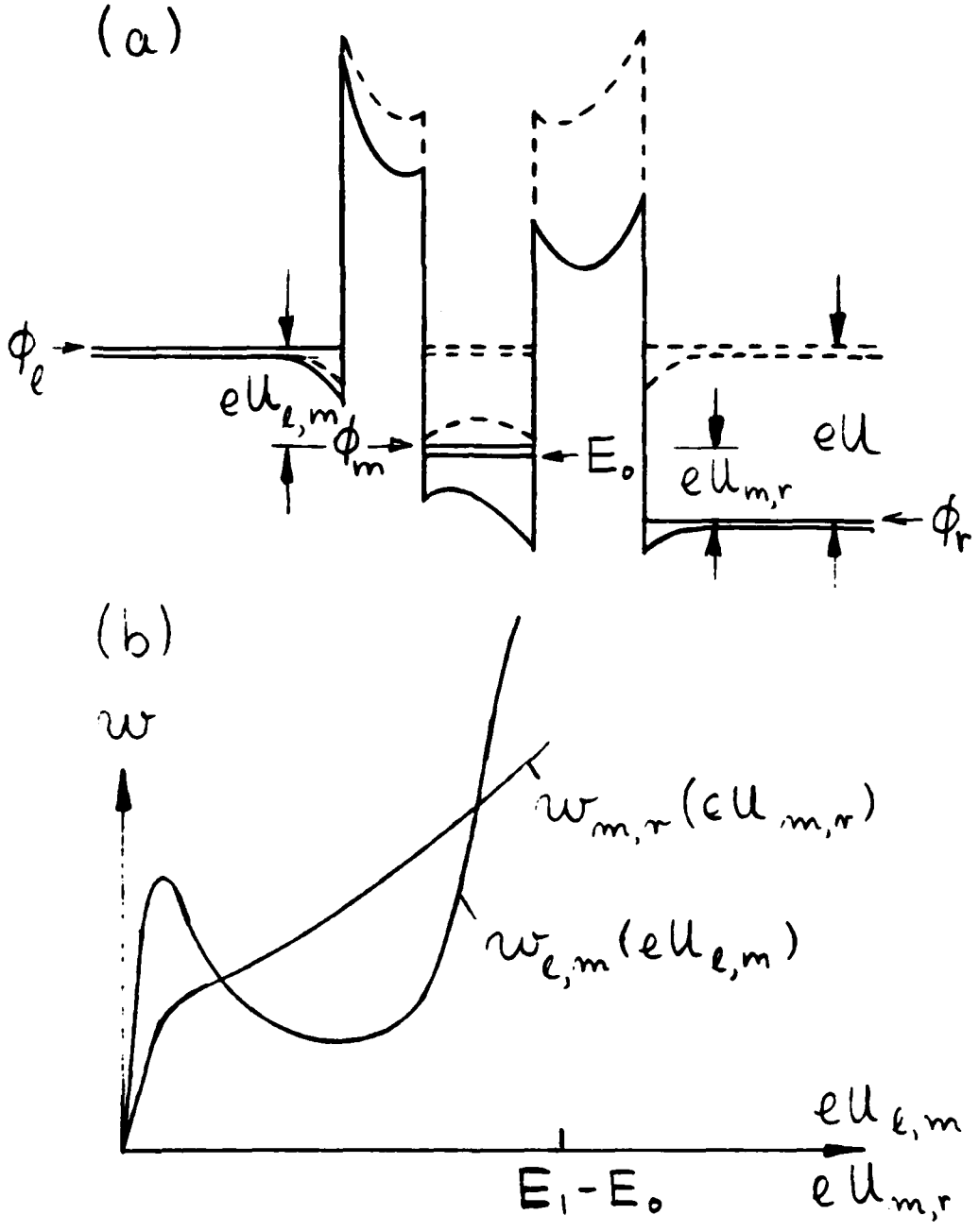
(a)
ϕ_ℓ
$eU_{\ell,m}$
ϕ_m
E_o
$eU_{m,r}$
eU
ϕ_r
(b)
w
$w_{m,r}(eU_{m,r})$
$w_{\ell,m}(eU_{\ell,m})$
$eU_{\ell,m}$
$E_1 - E_o$
$eU_{m,r}$

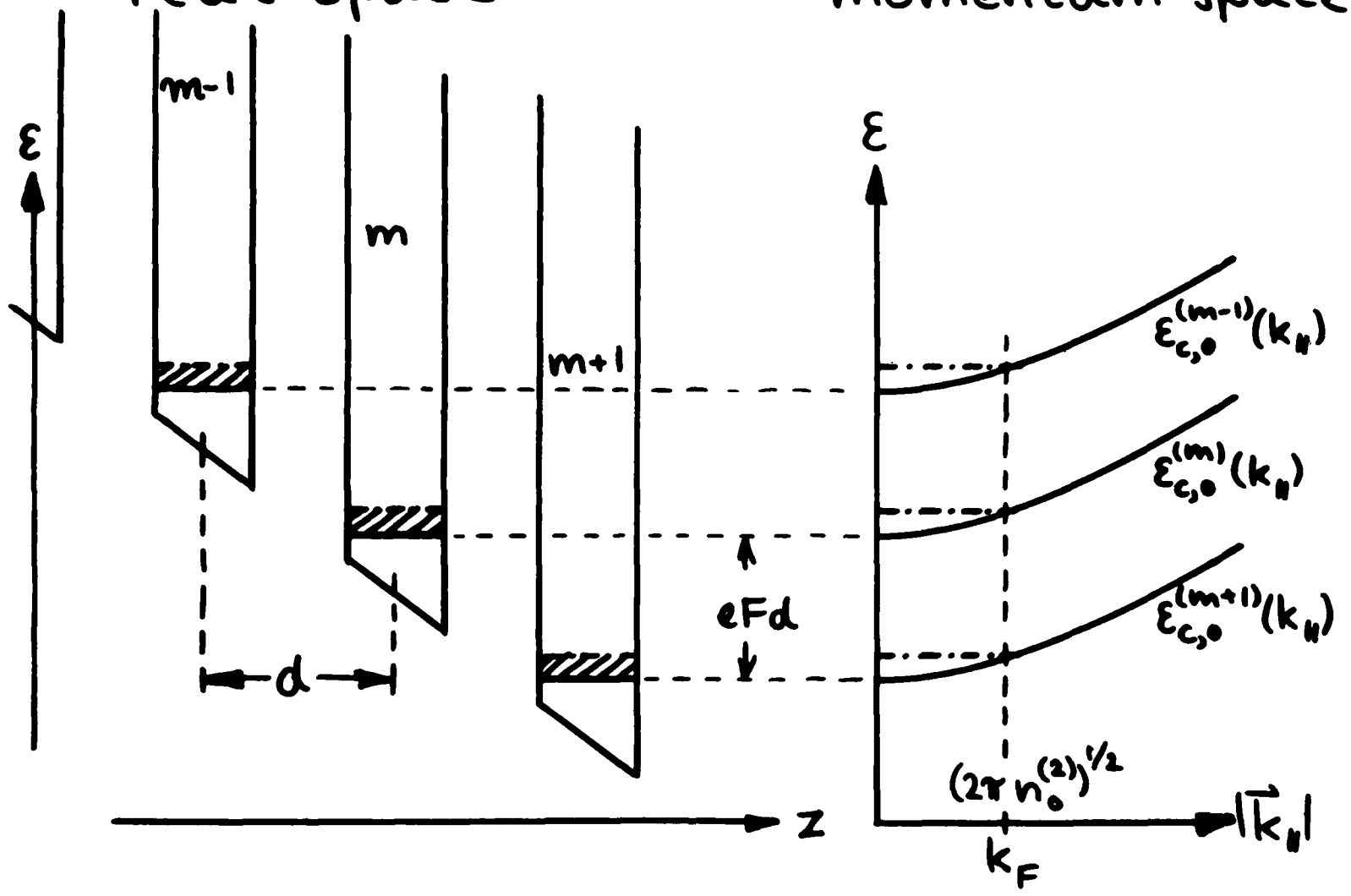
real space
momentum space
ε
m-1
m
m+1
d
eFd
z
$\varepsilon_{c,0}^{(m-1)}(k_\parallel)$
$\varepsilon_{c,0}^{(m)}(k_\parallel)$
$\varepsilon_{c,0}^{(m+1)}(k_\parallel)$
$(2\pi n_0^{(2)})^{1/2}$
k_F
$|\vec{k}_\parallel|$

Fig 12

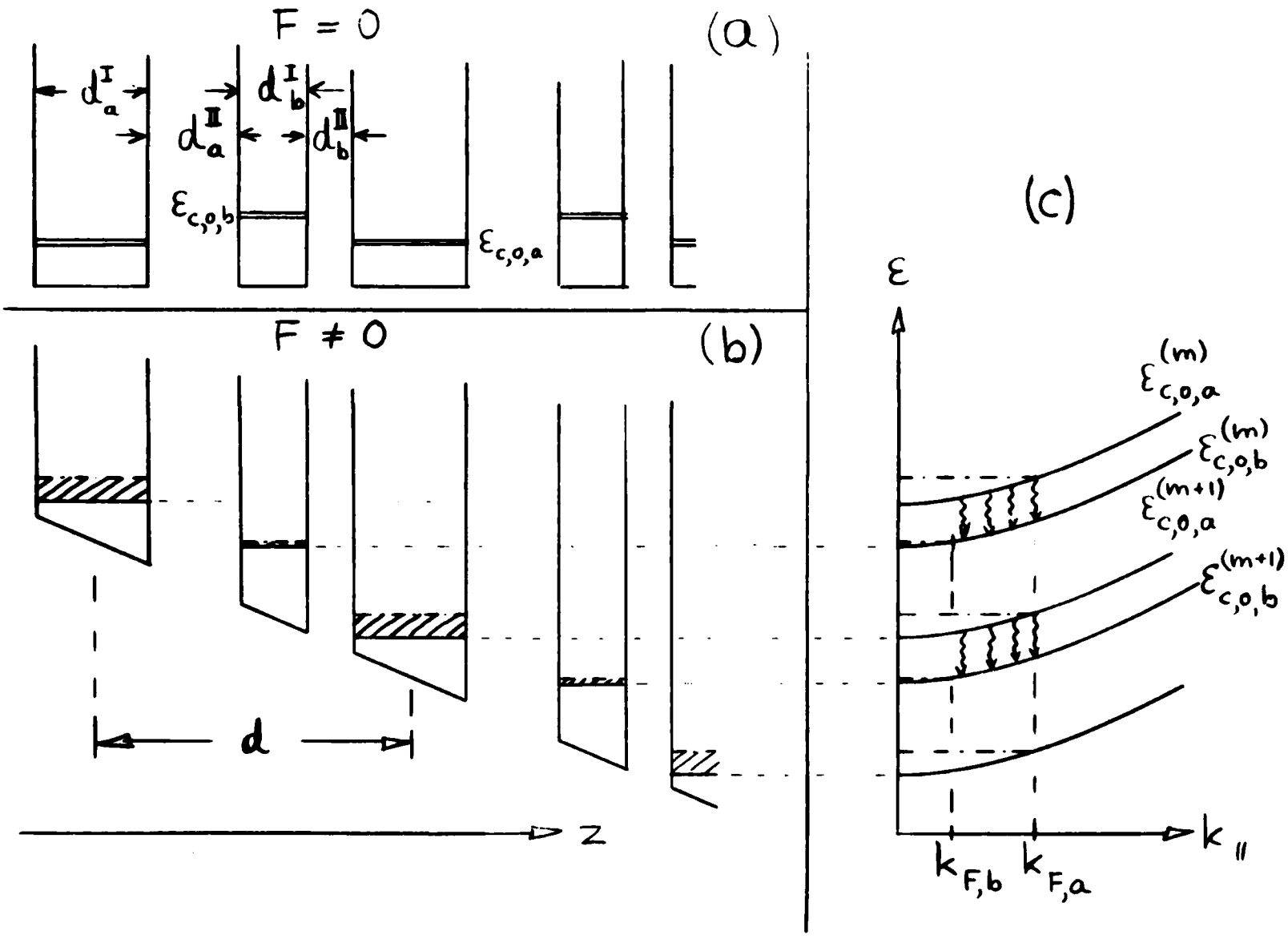
F = 0
(a)
d_a^I
d_b^I
d_a^{II}
d_b^{II}
$\varepsilon_{c,0,b}$
$\varepsilon_{c,0,a}$
F ≠ 0
(b)
d
z
(c)
ε
$\varepsilon_{c,0,a}^{(m)}$
$\varepsilon_{c,0,b}^{(m)}$
$\varepsilon_{c,0,a}^{(m+1)}$
$\varepsilon_{c,0,b}^{(m+1)}$
$k_{F,b}$
$k_{F,a}$
$k_{\parallel}$

Fig. 13

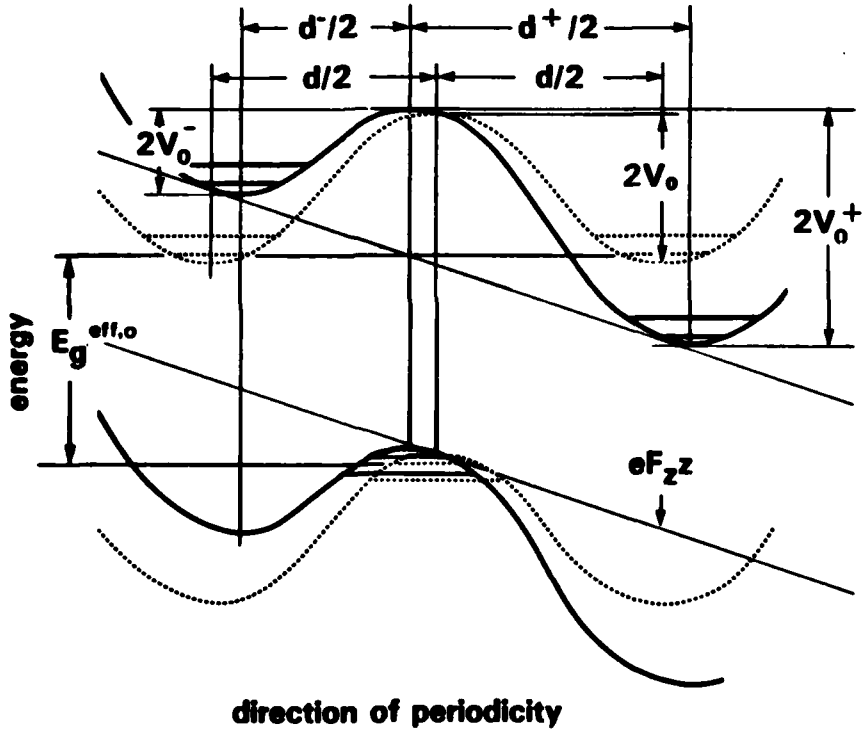
d⁻/2
d⁺/2
d/2
d/2
2V₀⁻
2V₀
2V₀⁺
E_g^eff,o
energy
eF_z z
direction of periodicity

END

FILMED

11-84

DTIC